Review Article

Polarising Agents and Spin Tags for Dynamic Nuclear Polarisation (DNP)-Enhanced Solid-State Nuclear Magnetic Resonance (ssNMR) Analysis of Biological Samples

ABSTRACT

Solid-state nuclear magnetic resonance (ssNMR) spectroscopy can obtain structural, functional and ligand-binding information about frozen and solid-like biological samples. ssNMR spectra can be enhanced by orders of magnitude using the technique of dynamic nuclear polarisation (DNP). In DNP there is polarisation transfer from high-gyromagnetic ratio (γ) unpaired electrons to neighbouring nuclei using microwave irradiation at or near the electron Larmor frequency. This produces an absolute increase in the signal-to-noise ratio and allows experiments on much smaller quantities of sample and/or using much shorter acquisition times. Along with necessary instrumentation an essential requirement for DNP-ssNMR is a sample with an endogenous free radical or an exogenous free radical polarising agent must be added to the sample. The polarising agent must be soluble in the sample matrix and compatible with the biological sample. The free radical(s) of the polarising agent also must be stable for the lifetime of DNP-ssNMR experiments. Nitroxides have been most used as polarising agents, including the biradical compounds TOTAPOL and AMUPol with a wide range of biological samples to produce DNP enhancement factors (ε) of up to 250. Derivatives of TOTAPOL and AMUPol and many other different polarising agents have also been used. Whilst conventional polarising agents are mixed throughout the sample, others are targeted at specific sites to provide a more localised signal enhancement. Here we review the different polarising agents and spin tags that have been used in DNP-ssNMR studies on biological samples.

Keywords: biological samples; dynamic nuclear polarisation; free-radical; microwave irradiation; polarising agent; signal enhancement; solid-state NMR

1. INTRODUCTION

Nuclear magnetic resonance (NMR) spectroscopy is a widely used and powerful analytical technique that can produce qualitative and quantitative chemical, structural and dynamic information from a wide range of samples including organic and inorganic compounds, pharmaceuticals, biomolecules and biological samples, food, industrial and environmental samples [1-13]. It is also the basis for the clinical technique of magnetic resonance imaging (MRI). Despite this, NMR is intrinsically an insensitive technique, typically requiring up to milligram quantities of sample and/or very long experiment times. The insensitivity originates from the fact that the size of the NMR signal is related to the relative populations of the magnetic energy levels being observed. At thermal equilibrium the energy levels are extremely close together, thus requiring very little energy for the nuclei to be promoted from one to the other. In the simplest case of a spin-½ nucleus with two magnetic energy levels, the Boltzmann distribution predicts that an almost equal number of nuclei will be in the higher and lower energy states. For example, the population difference between higher and lower states of hydrogen atoms is only around 1 in 10^5 spins, so the NMR signal is very weak. The sensitivity is significantly worse for all other NMR-active nuclei [1]. An improved signal-to noise-ratio has traditionally been achieved by increasing the concentration of

the sample, by acquiring and averaging a greater number of scans, by using a higher magnetic field to increase the energy difference between states or by using considerably lower probe and sample temperatures. There are limits as to what be achieved, especially for the biomolecules and biological samples that can only be obtained in low microgram quantities and that may not be stable for days to weeks of experiment time. The inherent insensitivity of NMR has been a major limiting factor for extending its application to larger and more complex biological samples, such as mem-brane proteins.

For target samples that are too large for efficient orientation averaging in solution, solid-state NMR (ssNMR) is employed, usually in combination with the method of magic-angle spinning (MAS) [14-23]. Fast rotation of the sample with frequencies up to ~100 kHz about an axis tilted 54.74° with respect to the external magnetic field results in collapse of most anisotropies and can produce isotropic NMR spectra like those in solution. A breakthrough in improving the sensitivity of ssNMR was the development of dynamic nuclear polarisation (DNP).

2. DYNAMIC NUCLEAR POLARISATION SOLID-STATE NMR

DNP is a powerful method for increasing the sensitivity of ssNMR by up to several orders of magnitude. It exploits polarisation transfer from high-gyromagnetic ratio (γ) unpaired electrons to neighbouring nuclei using microwave (MW) irradiation at or near the electron Larmor frequency. This leads to an absolute increase in the signal-to-noise ratio (S/N) and allows biological samples of much lower concentration to be studied in much shorter times (hours instead of days or weeks). Conventional DNP enhancement is defined as $\varepsilon \equiv I_{on}/I_{off}$ where I_{on} and I_{off} represent the NMR signal intensities with and without MW irradiation. In theory, a DNP enhancement factor, ε, equal to the ratio between the gyromagnetic ratios of the electron spin ($\gamma = 2.80249536 \times 10^4$) and the nuclear spin can be obtained. Theoretical enhancement factors from DNP are therefore up to ~660 for ^{1}H ($\gamma = 42.576$), ~2624 for ^{13}C ($\gamma = 10.705$) and 6511 for ^{15}N ($\gamma = 3.0766$) using Boltzmann electron spin polarisation.

The phenomenon of DNP first came from Overhauser (1953) [24], who proposed that transfer of polarisation from electrons to nuclei in metals was possible by saturating the electron transition, and this was experimentally verified in metals by Carver and Slichter (1953) [25]. During the 1980s, DNP was combined with MAS solid-state NMR (SSNMR) but extending DNP to higher fields proved challenging due to a lack of high-power MW sources [26-28]. Since then, the extension of DNP to high fields and the use of DNP for signal enhancement in solid-state NMR measurements on biological samples have been pioneered by Griffin and co-workers at the Francis Bitter Magnet Laboratory at Massachusetts Institute of Technology [29-46]. For DNP-enhanced measurements on biological samples, a water-soluble free radical compound or polarising agent was included in the frozen sample containing H_2O/glycerol and the biomolecule to be studied [47,48]. Most DNP-enhanced experiments are based on hyperpolarisation at cryogenic temperatures, followed by rapid dissolution and NMR measurements at ambient temperatures [49], or on DNP solid-state NMR with frozen samples under MAS [50-54], which are the focus of this review.

2.1 DNP transfer mechanisms

DNP is possible in the liquid-state, but it is generally much less efficient because of diminished intermolecular dipolar couplings due to fast molecular tumbling [55,56]. The only practical mechanism available to directly polarise liquids is the Overhauser effect, involving dipolar relaxation between electrons and nuclei [57]. The Overhauser effect occurs with mobile electrons in gases and liquids and in conducting solids, but it is less efficient at higher magnetic fields. Approaches for performing DNP on liquid samples include use of supercritical solvents, polarisation at low magnetic field followed by NMR measurement at high magnetic field, or polarisation of a solid/frozen sample followed by rapid dissolution/in-situ melting and NMR measurement with enhanced polarisation in the liquid-state [58,59].

For DNP in the solid-state, three principal mechanisms have been proposed for polarisation transfer from electrons to neighbouring nuclei: (i) solid effect and (ii) cross effect mechanisms, based on quantum mechanics and relaxation on small spin systems, and (iii) thermal mixing mechanism, which originates from the thermodynamic macroscopic notion of spin temperature [39, 60] (Fig. 1).

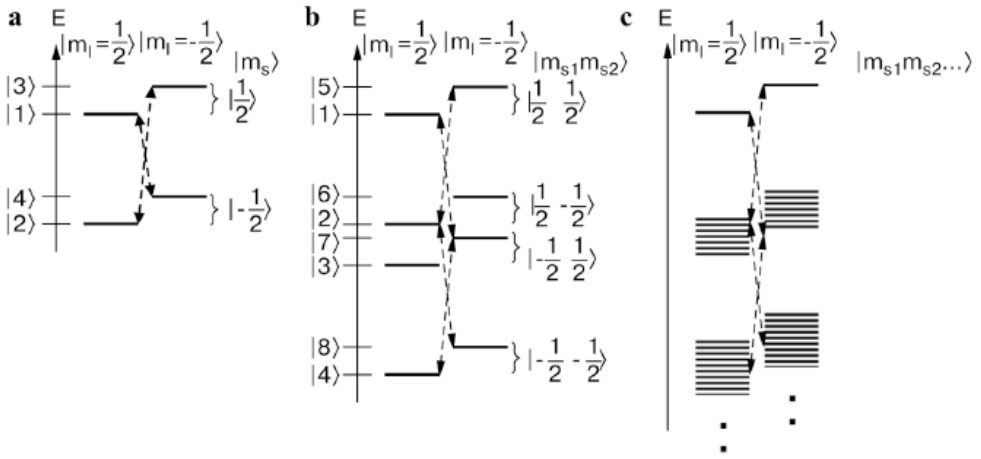

Fig. 1. Quantum mechanical diagrams of the electron-nuclear transitions (dashed arrows) in the spin effect (a), cross effect (b) and thermal effect (c) mechanisms, which involve single, paired and multiple electron spins, respectively. This figure was reproduced from Barnes et al. (2008) [39].

The solid effect mechanism involves one electron spin and nuclear polarisation enhancement results from irradiation of "forbidden" double quantum (DQ) or zero quantum (ZQ) electron-nuclear transitions that become allowed due to electron-nuclear hyperfine interactions [61,62]. The solid effect mechanism is dominant in systems where the polarising agent exhibits a homogeneous electron paramagnetic resonance (EPR) linewidth (δ) and an inhomogeneous spectral breadth (Δ) smaller than the nuclear Larmor frequency (δ, Δ< ω0I). This condition is satisfied by radicals with high molecular symmetry [63-65]. Because the solid effect mechanism requires a polarising agent with a relatively narrow EPR spectrum, this restricts its practical applicability in DNP-enhanced measurements [38].

The cross effect mechanism requires at least a three-spin system composed of two electrons and a nucleus and for this process to occur the difference between the electron Larmor frequencies of these two electrons must be about equal to the nuclear (^{1}H) Larmor frequency (ω0e1 – ω0e2 = ±ω0^{1}H). This results in strong state mixing and there is a high probability that MW irradiation resonant with electron 1 will flip electron 2 and the coupled proton together [66-69]. Hence, cross effect operates when the polarising agent has an inhomogeneous broadened EPR spectrum whose breadth is larger than the nuclear Larmor frequency ω0I, and therefore the homogeneous linewidth δ remains small (Δ > ω0I > δ) [38]. High-field cross effect DNP experiments were initially performed with mono-radical species, such as TEMPO (**1**) [31,32]. In this case the frequency matching condition is fulfilled only for the fraction of the radicals that adopt the correct relative orientation of their g-tensors. Improvement in cross effect DNP was made by using biradicals [33,35] consisting of two tethered TEMPO moieties that achieve relatively short (~12 Å) electron-electron distances independent of concentration. Cross effect is the dominant continuous wave mechanism at high magnetic fields.

The thermal mixing mechanism involves multiple electron spins in the polarisation transfer and takes place when the characteristic EPR linewidth (δ) is in the order of or larger than the nuclear Larmor frequency. Here the electron-nuclear spin system can be described as a set of three interacting baths, each characterised by a spin temperature: electron Zeeman system (EZS), electron dipolar system (EDS), nuclear Zeeman system (NZS) [38]. Off resonance irradiation of the allowed EPR transition results in a large polarisation gradient across the EPR line, which is equivalent to cooling the EDS. This bath is in thermal contact with the NZS, which is also cooled in an energy-conserving three-spin electron-electron-nuclear exchange, leading to DNP enhancement. At the high fields and low temperatures (80–110 K) typically used in MAS experiments, thermal mixing does not provide an important polarisation pathway.

For comprehensive descriptions of theory behind the proposed DNP transfer mechanisms see Barnes et al. (2008), Maly et al. (2008), Corzilius et al. (2012), Hovav et al. (2012), Ni et al. (2013), Mentink-Vigier et al. (2015), Corzilius, (2016), Ravera et al. (2016), Lilly Thankamony et al. (2017) [38,39,43,57,60,70-73] and references within.

2.2 Components for DNP-SSNMR

The essential components required for performing DNP-ssNMR are an NMR magnet with a low-temperature MAS NMR probe that allows simultaneous irradiation of the sample with MW (THz) and radiofrequency power, a high-power MW/THz source such as a gyrotron oscillator, a low-loss transmission line that delivers continuous THz power from the source to the sample, and a free radical polarising agent (Fig. 2). The polarising agent can be either an endogenous radical in the

sample or an exogenous radical that is added to the sample. The efficiency of polarisation transfer is dependent on the structure and properties of the polarising agent.

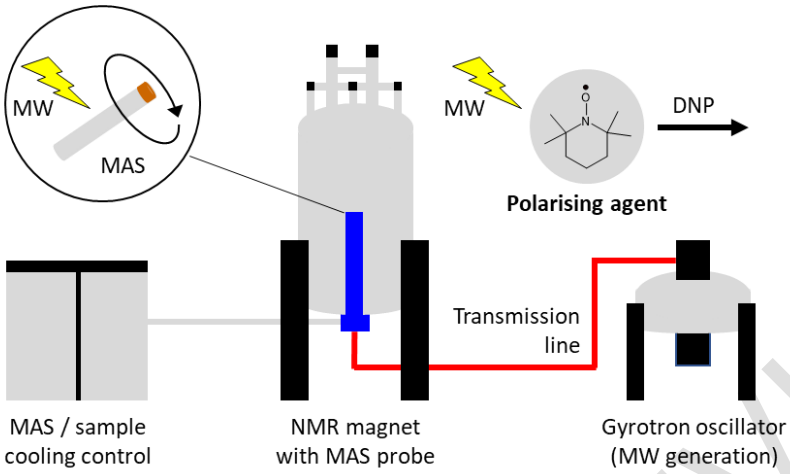

Fig. 2. Components for DNP-ssNMR.

3. POLARISING AGENTS FOR DNP-SSNMR ANALYSIS OF BIOLOGICAL SAMPLES

Because appropriate endogenous free radicals are not commonly found in biological samples, exogenous free radical polarising agents usually must be added to samples for DNP-ssNMR. In addition to providing efficient nuclear polarisation, there are additional factors to consider for polarising agents with biological samples. The desired concentration range of the polarising agent in the sample is typically 5-20 mM and the sample is usually frozen at low temperatures, typically 80-120 K (Table S1). The sample and polarising agent are usually dissolved in or mixed with a cryoprotecting agent, the most common being a glycerol/water mixture that produces a glassy matrix when frozen. The polarising agent therefore needs to be soluble at the desired concentration in this mixture. Deuterated components can be used for higher DNP efficiency, and a d_8-glycerol/D_2O/H_2O cryoprotectant mixture is sometimes referred to as “DNP juice”. An exogenous polarising agent ideally needs to be mixed uniformly in the sample. The polarising agent needs to be compatible with the biological sample, in that it does not adversely affect its native structure and function. The radical(s) of the polarising agent also need to be stable in the biological sample/matrix and remain stable for the lifetime of DNP-ssNMR experiments. This is especially challenging for applying DNP to cells and cell-derived samples, where there can be fast reduction of radicals by native antioxidants from the cellular environment. Appropriate tests and control experiments should be performed to assess the usefulness and compatibility of chosen polarising agents with biological samples.

Nitroxides are most used as exogenous polarising agents for DNP-ssNMR due to their stability in biological systems. A major development in polarising agents was the introduction of nitroxide biradicals with much better nuclear polarisation. These biradicals satisfy the requirement of having two strongly coupled electron spins for DNP through the cross-effect mechanism. The biradical polarising agents TOTAPOL and AMUPol (see below) have been most used and have also been modified to improve their water solubility, to increase their molecular weight and to contain rigid linkers, and methyl groups adjacent to nitroxides have been replaced. Nitroxide-containing compounds begin the present review of polarising agents that have been used in DNP-ssNMR studies on biological samples.

3.1 TEMPO and derivatives

The mono-radical TEMPO (2,2,6,6-tetramethyl-1-piperidinyloxy) (**1**) was used as the polarising agent in the first application of DNP-ssNMR to study the functional intermediates of a protein. TEMPO was used a concentration of 40 mM in samples of [ζ-^{15}N]lysine-labelled bacteriorhodopsin purple membrane to give DNP signal enhancements of up to $\varepsilon = 40$ [74]. This enabled the first NMR observation of the K intermediate of the ion-motive photocycle of bacteriorhodopsin and confirmed the identification of the NMR signals of several L intermediates.

TEMPO and the derivatives TEMPOL (4-hydroxy-TEMPO) (**2**) and TEMPONE (4-oxo-TEMPO) (**3**) at a concentration of 100 mM were used as the polarising agent in aqueous samples of the small ^{13}C-labelled biological molecules serine, alanine, glycine, proline, glucose, indole and imidazole in Overhauser DNP (ODNP) measurements at high field (9.4 T) and at room temperature. In these liquid-state experiments the electron-nucleus polarisation transfer is mediated by the electron-nucleus Overhauser effect driven by molecular motions, which achieved DNP enhancements of up to $\varepsilon = 11$ [75].

Heparins with TEMPO groups heterogeneously distributed along the heparin back-bone have been tested as potential polarising agents for DNP-ssNMR. The spin-labelled heparins provided ^{1}H DNP enhancement factors of up to ε = 110 [76].

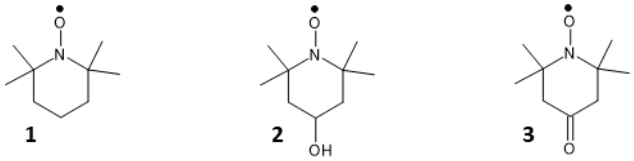

3.2 TOTAPOL

The first widely used polarising agent for DNP-ssNMR on biological samples was the biradical compound TOTAPOL (1-[(2,2,6,6-tetramethyl-1-oxidopiperidin-4-yl)amino]-3-(2,2,6,6-tetramethyl-1-oxopiperidin-1-ium-4-yl)oxypropan-2-ol or 1-(TEMPO-4-oxy)-3-(TEMPO-4-amino)propan-2-ol) (**4**), which comprises two molecules of TEMPO tethered by 3-aminopropane-1,2-diol. In the first report of the synthesis and characterisation of TOTAPOL [35], a 6 mM concentration of TOTAPOL affected an enhancement factor of ε = 240 for DNP (5 T, 90 K, 140 GHz µWave) on [U-^{13}C, ^{15}N]proline in aqueous media. Being compatible with aqueous media is clearly an important property for polarising agents in DNP-ssNMR studies on many biological samples.

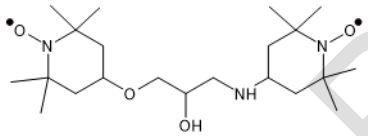

4

Since 2006, TOTAPOL has successfully been used at concentrations of 2.5-60 mM as the polarising agent for DNP-ssNMR studies on a wide range of biological samples (Table S1). These include amyloid fibrils [77-81], light-harvesting complex bacteriorhodopsin [82], SH3 domain of α-spectrin [83], neurotoxin II bound to acetylcholine receptors in native membranes [84], signal peptide bound to lipid-reconstituted Sec translocon [85], plant (*Arabidopsis thaliana*) and bacterial (*Bacillus subtilis*) cell walls [86,87], bovine serum albumin [88], lung surfactant peptide KL4 [89], disulfide oxidoreductase A (DsbA) signal peptide in the exit tunnel of the ribosome [90], and mammalian P450-cytochrome b5 complex in lipid bilayers [91]. Also, various transport proteins (M2 proton transporter from influenza A virus, EmrE multidrug efflux pump, potassium channel KcsA) [92-94] and viral capsids from HIV-1 and bacteriophage AP205 [95].

In these studies using TOTAPOL, the DNP enhancement factor ranged from ε = 1.7 to 160 (Table S1). For example, a DNP-ssNMR study of purified amyloid fibrils of the prion domain of the yeast prion protein Sup35 in cell lysate achieved up to 115-fold signal enhancements in ^{13}C spectra using 10 mM TOTAPOL. This enabled detection of the protein at endogenous levels in a complex physiological environment and investigation of the structural influence of cellular lysates on amyloid fibril assembly (Fig. 3) [81].

It is important to consider the stability and therefore the longevity of polarising agents in biological samples. That is to say, the radical must remain active for at least the time it takes to mix it with the sample, insert the sample into a rotor and freeze, which could be up to an hour. A study on the stability of TOTAPOL demonstrated that it is quickly (minutes) reduced in *Escherichia coli* cell pellets, suspensions and lysates. But fortunately, treatment of cells with the cysteine blocker *N*-ethylmaleimide significantly slowed the rate of reduction, and treatment of lysates with potassium ferricyanide completely re-oxidised the reduced TOTAPOL [96].

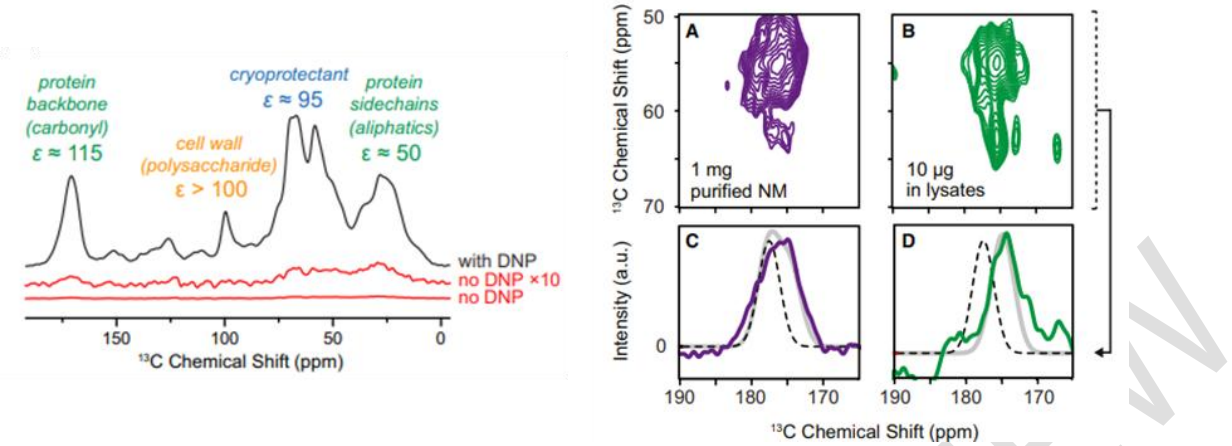

Fig. 3 legend. Left. One-dimensional $^{13}C\{^{1}H\}$ spectra of purified amyloid fibrils of the prion domain of the yeast prion protein Sup35 in cell lysate both with (black) and without (red) DNP enhancement by microwaves. DNP gave large signal enhancements (ε) for uniformly $^{1}H,^{13}C$-labeled NM in a deuterated matrix of cellular lysates containing a 60:30:10 (v/v) mixture of d_8-glycerol:D_2O:H_2O and 10 mM TOTAPOL (**4**) at 211 MHz/140 GHz with $\omega/2\pi$ = 4.3 kHz and a sample temperature of 83 K. Right. (A and B) Carbonyl carbon region of ^{13}C-^{13}C correlation spectra at 700 MHz using DNP MAS NMR of (A) cryoprotected purified Sup35 fibrils acquired in 6 hours and (B) cryoprotected Sup35 fibrils assembled in the presence of cellular lysates acquired in 1 week. (C and D) Examination of the carbonyl carbon (C′) region of the spectra in projections of the Cα region (50–70 ppm indicated by dotted bracket) reveals the secondary structural composition of the protein backbone. The projection eliminates signals from non-backbone sites, such as the carbonyl moieties in the amino acid side chains like Asn and Gln. Dotted black lines indicate the expected chemical shift values for α-helical conformations of the protein backbone and highlight a large shift away from α-helical character for Sup35 fibrils in lysates (D). The grey line represents the best-fitted solution to three Gaussian distributions describing the expected chemical shifts for the three possible secondary structural motifs: α helices (177.8 ± 1.5 ppm), random coils and turns (175.6 ± 1.5 ppm) and beta sheets (175.4 ± 1.55 ppm). Fits to a sum of these three Gaussian distributions gave standard estimates of error of 0.84 (C) and 0.93 (D). This figure was adapted from Frederick et al. (2015) [81].

3.3 AMUPol

The biradical polarising agent AMUPol (15-{[(7-oxyl-3, 11-dioxa-7-azadispiro [5.1.5.3] hexadec-15-yl) carbamoyl] [2-(2,5,8,11-tetraoxatridecan-13-ylamino)}-[3,11-dioxa-7-azadispiro [5.1.5.3] hexadec-7-yl]) oxidanyl) (**5**) was introduced as a more efficient and more water soluble alternative to the established agent TOTAPOL [97]. AMUPol was synthesised in four steps from 1,2,2,6,6-pentamethylpiperidin-4-one and it showed DNP enhancements of 3.5 to 4 times greater than for TOTAPOL. AMUPol has emerged as by far the most used polarising agent for biological samples with DNP enhancement factors ranging from ε = 16 to 250 (Table S1).

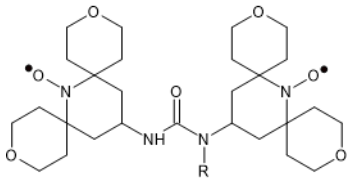

5 R = $(CH_2CH_2O)_4CH_3$

For example, a DNP-ssNMR study used AMUPol as the polarising agent for determining the cholesterol binding site of eukaryotic membrane proteins in native-like membranes [98]. The approach involved yeast biosynthetic ^{13}C-labelling of cholesterol, in this case using [1-^{13}C]glucose to preferentially label methyl carbons, and detection of ^{13}C-^{13}C cross peaks with the ^{13}C-labelled protein in 2D correlation spectra under DNP conditions at 110 K. This was demonstrated on the influenza M2 protein (residues 21-97), which was site-specific $^{13}C,^{15}N$-labelled at Ile, Phe, Gly, and Ala residues and reconstituted in POPC/POPG bilayers. The use of 15 mM AMUPol produced DNP enhancements of ε = 28 to 42, which allowed detection of multiple cross peaks between cholesterol and M2 in double quantum filtered 2D ^{13}C-^{13}C spectra, measurement of distance restraints, and molecular docking of cholesterol on M2 (Fig. 4) [98].

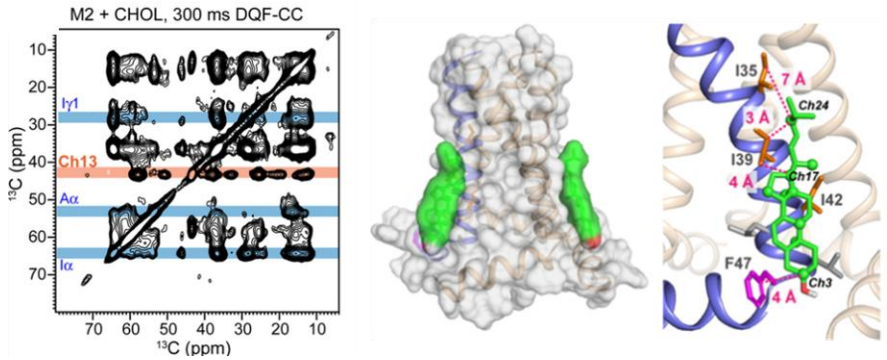

Fig. 4. Left. Example 2D DQF-CC spectrum of site-specific labelled M2 and [1-^{13}C]glucose-labelled cholesterol in POPC/POPG membranes with 15 mM AMUPol (**5**) measured at 110 K with DNP and a ^{13}C spin diffusion mixing time of 300 ms. DQF significantly simplifies the ω1 dimension of the spectra, facilitating assignment of intermolecular protein-cholesterol cross peaks. Right. Cholesterol (green) docking onto M2 (PDB code: 2L0J) using HADDOCK. Distance restraints obtained from the 2D ^{13}C-^{13}C spectra were used to constrain the binding site. Cholesterol carbons that exhibit cross peaks with the M2 protein are shown as spheres. Key Ile and Phe residues at the binding interface are indicated, along with the distances to the cholesterol carbons. This figure was adapted from Elkins et al. (2018) [98].

AMUPol was used as the polarising agent in an elegant DNP-ssNMR study on the pentameric light-driven proton pump green proteorhodopsin, which enabled observation of light-dependent, functionally relevant cross talk between protomers of the proteorhodopsin homo-oligomer [99]. The study used wild-type and mutant forms of proteorhodopsin site-specific labelled with [$^{13}C_6$, $^{15}N_3$]histidine, [^{15}Nε]lysine and [^{13}Cδ1]tryptophan reconstituted in DMPC/DMPA lipids and containing 20 mM AMUPol, which produced DNP enhancement factors of ε = 40 to 60. Proteorhodopsin was trapped in different photointermediate states by using cryogenic temperatures, for example, the K state was trapped by illuminating the wild-type form directly in the DNP-NMR probe at 100 K. The M state was trapped by illumination of the E108Q mutant at room temperature directly inside the MAS rotor followed by fast freezing in liquid nitrogen. A highly conserved histidine residue (His75) is located at the protomer interface, and this was exploited in various DNP-ssNMR experiments detecting cross-protomer contacts (Fig. 5). It was shown that His75 switches from the (τ)- to the (π)-tautomer and changes its ring orientation in the M state. His75 couples to a tryptophan residue (Trp34) across the oligomerization interface and defines a cross-protomer Asp–His–Trp triad, which potentially serves as a pH-dependent regulator for proton transfer [99].

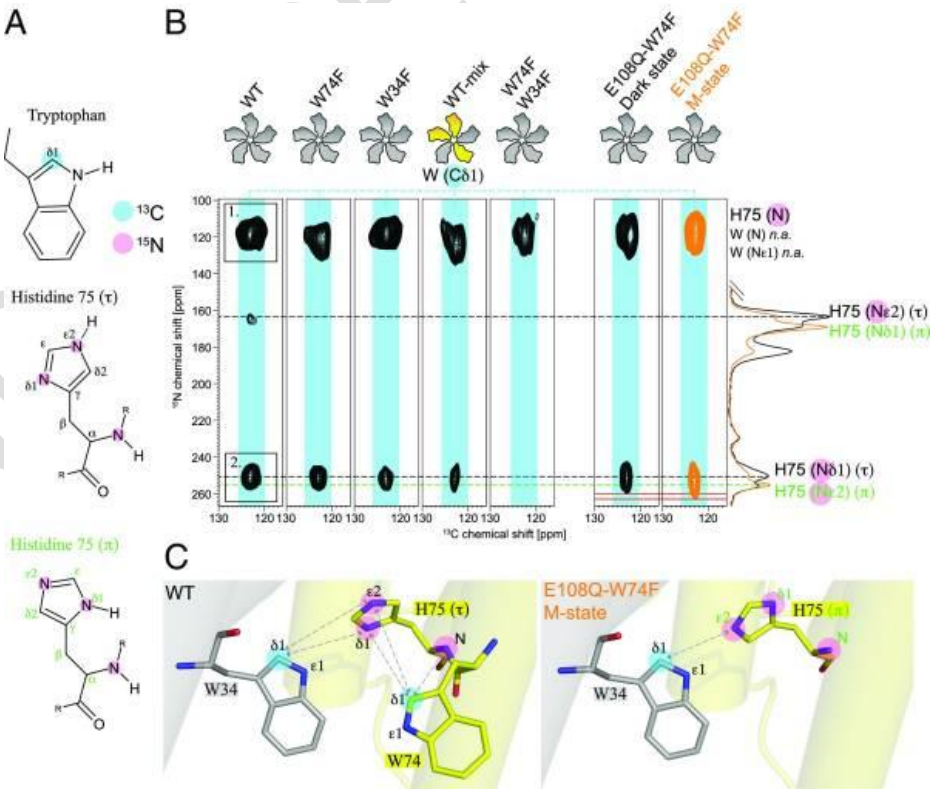

Fig. 5. Visualising the cross-protomer H75-W34 contact in green proteorhodopsin. (A) For the detection of the cross-protomer H75-W34 contact, (^{13}Cδ1-Trp, ^{15}N3-His)-GPR$_{WT}$ (wild type) and various mutants were prepared. (B) Two-dimensional TEDOR spectra of GPR$_{WT}$, GPR$_{W74F}$, GPR$_{W34F}$, GPR$_{WT\text{-}mix}$, GPR$_{W74F\text{-}W34F}$, and GPR$_{E108Q\text{-}W74F}$, all with (^{13}Cδ1-Trp, ^{15}N3-His) labelling. The 1D spectra on the right are from ($^{13}C_6$-^{15}N3-His, ^{15}Nε-Lys)-GPR$_{E108Q}$ in the dark state (black) and M state (orange) and were plotted to identify the H75(τ) and (π) resonances. Cross peak 1 in GPR$_{WT}$ (left) is observed in all spectra and corresponds to a mixture of correlations between W34/W74-Cδ1 and H75-N as well as natural abundance correlations between Trp-Cδ1 and Trp-N or Trp-Nε1. Cross peak 2 can be attributed to a correlation between W74 or W34-Cδ1 and H75-Nδ1(τ). Spectra of GPR$_{W74F}$ and GPR$_{W34F}$ confirm that both tryptophan residues contribute to the interaction. The mixed-labelled sample GPR$_{WT\text{-}mix}$ consisting of (^{13}Cδ1-Trp)-GPR$_{WT}$ and (^{15}N3-His)-GPR$_{WT}$ proves that a W34-H75 interprotomer contact exists. M state trapping of (^{13}Cδ1-Trp, ^{15}N3-His)-GPR$_{E108Q\text{-}W74F}$ shows a stretching of signal 2 toward the Nε2(π) resonance. (C) The GPR$_{WT}$ sample shows close proximity of H75-Nδ1(τ) to W34-Cδ1 and an intraprotomer contact to W74-Cδ1. The GPR$_{E108Q\text{-}W74F}$ sample indicates a turn of H75 so that Nε1(π) and W34-Cδ1 occur in close proximity. This figure was reproduced from Maciejko et al. (2019) [99].

A recent study on the stability of AMUPol in intact and lysed mammalian cells showed that AMUPol was reduced at a slower rate than TOTAPOL. Indeed, the reduction of AMUPol by mammalian cell lysates was slow relative to the time scale of cellular sample preparation for DNP-ssNMR [100]. Like for TOTAPOL [96], reduction of AMUPol was prevented by 2.5 mM *N*-ethylmaleimide, but this also compromised cellular viability and did not improve DNP performance. It was suggested that the most effective approach to achieve high DNP enhancements for samples of cells is to minimise room temperature contact times with cellular constituents.

3.4 Derivatives of TOTAPOL and AMUPol

Some highly water-soluble derivatives of TOTAPOL and AMUPol were introduced in which the four ring-oxygens of AMUPol were replaced with a carbon atom and a hydroxyl group attached at each of these positions. bcTol [bis(spirocyclohexyl-TEMPO-alcohol)urea] (**6**) [101] and bcTol-M [bis(spirocyclohexyl-TEMPO-alcohol)-ureadimethyl] (**7**) [102] both retain the carbamide group of AMUPol, which is unsubstituted or substituted with methyl groups in the two molecules, respectively. In cyolyl-TOTAPOL [spirocyclohexanol-yl-1-(TEMPO-4-oxy)-3-(TEMPO-4-amino) propan-2-ol] (**8**), the carbamide group is replaced by the 3-aminopropane-1,2-diol group of TOTAPOL [102]. At a concentration of 20 mM, bcTOL has been used as the polarising agent in DNP-ssNMR studies of the functional sensory module of the cyanobacterial phytochrome Cph1 [103] and microcrystalline SH3 domain [101], with the latter achieving a DNP enhancement factor of $\varepsilon = 224$. bcTOL-M has been added from a stock concentration of 39.5 mM to K7M2 mouse osteosarcoma extracellular matrix enriched in ^{13}C, ^{15}N-amino acids to achieve a DNP enhancement factor of $\varepsilon = 26 \pm 9$ [104].

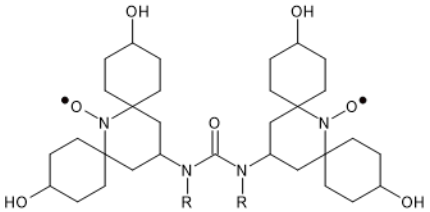

6 bc-Tol R = H
7 bc-Tol-m R = CH_3

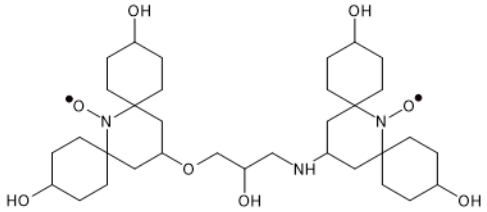

8

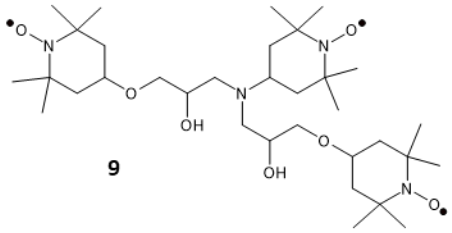

9

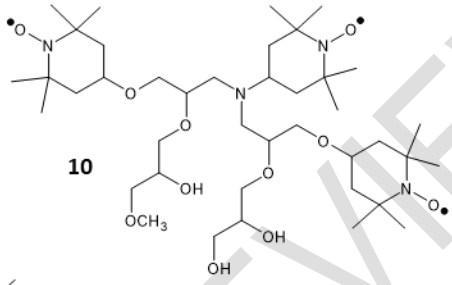

10

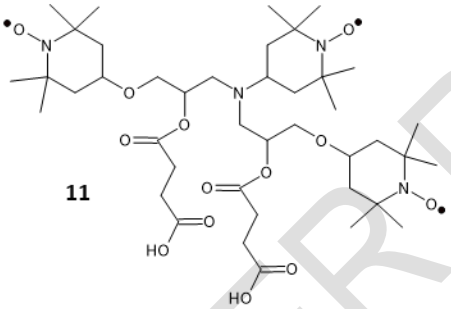

11

The triradical DOTOPA-TEMPO (4-[N,N-di-(2-hydroxy-3-(TEMPO-4'-oxy)-propyl)]-amino-TEMPO) (**9**) [105] was synthesised based on the procedure for TOTAPOL [35], but modified by reacting 4-amino-TEMPO and 4-(2,3-epoxypropoxy)-TEMPO in 1:1.7 ratio, instead of a 1:1 ratio. DOTOPA-TEMPO at 6 mM was used as the polarising agent in static DNP-ssNMR experiments at ultra-low temperature (8 K) on ^{13}C-labelled 40-residue β-amyloid samples in both fibrillar and non-fibrillar states. DNP signal enhancement factors of ε = 16-21 were achieved and this allowed use of 2D ^{13}C-^{13}C exchange spectroscopy to probe peptide backbone torsion angles (ϕ,ψ) in selectively ^{13}C-labeled β-amyloid [106]. The triradical DOTOPA-3OH-Methoxy (**10**) was synthesised from DOTOPA-TEMPO [107] and used as the polarising agent at 6 mM in DNP-ssNMR experiments on frozen solutions of Aβ40 amyloid fibrils at 25 K [108]. This achieved DNP enhancement factors of ε = 18-80 and enabled characterisation of successive stages of amyloid-β self-assembly. A DOTOPA derivative with much greater solubility in glycerol/water solutions at neutral and basic pH, succinyl-DOTOPA (4-{N,N-di-[2-(succinate, sodium-trimethylamine salt)-3-(TEMPO-4'-oxy)-propyl]}-amino TEMPO) (**11**), was synthesised by reacting DOTOPA with succinic anhydride [109]. The potential application of succinyl-DOTOPA as a polarising agent was demonstrated using 10 mM in DNP-ssNMR measurements at 25 K on a frozen solution of the 27-residue peptide M13 (uniformly ^{15}N, ^{13}C-labelled at Phe8, Ile9, Ala10, and Val11) with the calcium-sensing protein calmodulin. In 1D ^{13}C spectra, this achieved a DNP enhancement factor of ε = ~140 [109].

3.5 bTbK and derivatives

The conformationally-restricted biradical bTbK (**12**) was used as the polarising agent in DNP-ssNMR measurements on oriented samples of a ^{15}N-labelled transmembrane peptide in POPC membranes at 100 K, achieving a DNP enhancement factor of ε =18 [110]. A larger derivative of bTbK, known as TEKPol (**13**), was used as the polarising agent in DNP-ssNMR measurements on wild spider silks at 110 K. A concentration of 10 mM TEKPol produced DNP enhancements of ε = >50, which enabled the detection of novel hydrogen-bonding networks and arginine conformations, and the post-translational modified amino acid hydroxyproline [111]. The bulky and conformationally-restricted biradical polarising agent SPIROPOL (**14**) contains four sulphur atoms that exist as a mixture of sulphonyls, sulphoxides and thioethers [112]. SPIROPOL was tested alongside TOTAPOL as a polarising agent in DNP-ssNMR studies on sedimented samples and concentrated frozen solutions of bovine serum albumin. Under comparable conditions, TOTAPOL and SPIROPOL produced DNP enhancement factors of ε = 31 and 26, respectively [88].

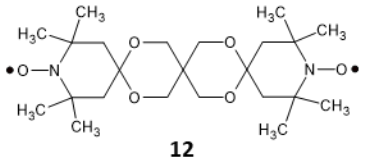

12

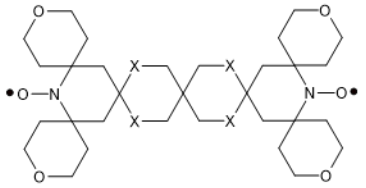

14 X = S / S=O / O=S=O

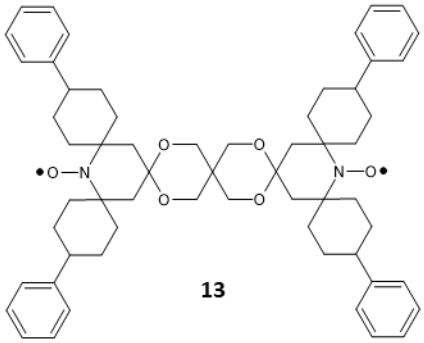

13

3.6 AsymPols and POPAPOL

A family of highly efficient biradical polarising agents known as AsymPols, which are composed of asymmetric bis-nitroxides, in which a piperidine-based radical and a pyrrolinoxyl or a proxyl radical are linked together, were computationally designed and then synthesised. The basic AsymPol agent (**15**) was modified by replacing the methyl groups by spirocyclohexanolyl groups to slow the electron spin relaxation, and phosphate groups were added to improve the solubility and to give the agent AsymPolPOK (**16**) [113]. A study of nitroxide biradicals for DNP in cellular environments compared the efficiency and stability of AsymPolPOK with TOTAPOL, AMUPol and also the pyrrolidine-based agent POPAPOL [1-(PROXYL-3-oxy)-3-(PROXYL-3-amino)propan-2-ol] (**17**).

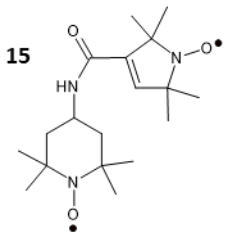

15

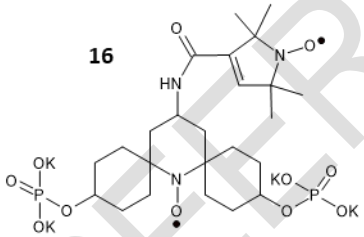

16

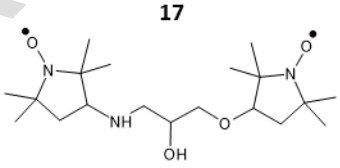

17

Using samples of [^{13}C,^{15}N]-proline in 60% d_8-glycerol, 30% D_2O, 10% H_2O with 10-15 mM polarising agent, POPAPOL, TOTAPOL, AMUPol and AsymPolPOK produced enhancements of ε = 32, 36, 160 and 72, respectively, in ^{13}C spectra at 14.1 T and 100 K (Fig. 6) [114]. At a concentration of 1 mM the same polarising agents produced enhancements of ε = 16, 10, 54 and 46, respectively. When the stability of the radicals was compared by EPR under reducing conditions in the presence of 1 mM ascorbic acid, POPAPOL had the slowest rate of reduction with a decay constant (τ) of 8.7 minutes, while the constant for TOTAPOL was 3.2 minutes. Interestingly, in mammalian HEK293 cell lysates, AsymPolPOK had the best DNP performance and stability [114]. AsymPolPOK was used as the polarising agent to achieve DNP enhancements of ε = >100 in ^{13}C spectra of polyglutamine amyloid fibrils, which enabled ^{13}C-^{13}C correlation experiments at natural abundance on 1-2 mg of sample [115].

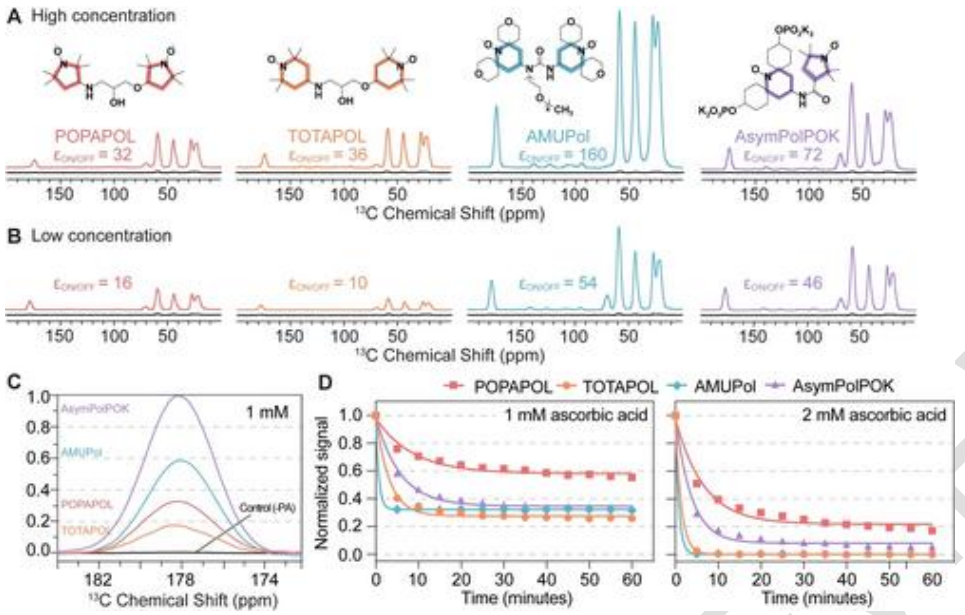

Fig. 6. Polarising agent performance in vitro. (A) DNP enhancements of 0.25 M $^{13}C,^{15}N$-labeled proline with 10 mM (AsymPolPOK and AMUPol) or 15 mM (TOTAPOL and POPAPOL) polarising agent. (B) DNP enhancements of 0.1 M $^{13}C,^{15}N$-labeled proline with 1 mM polarising agent. (C) Enhancement of the proline carbonyl signal of samples prepared with 1 mM polarising agent compared to a proline sample prepared without polarising agent. (D) Polarising agent (1 mM) reduction time course in 1- or 2-mM ascorbic acid, recorded by EPR. ϵ = enhancement. Standard error bars are shown, n=3. This figure was reproduced from Ackermann et al. (2022) [114].

3.7 TinyPols

The DNP enhancement efficiency of binitroxide polarising agents such as AMUPol drops significantly at higher magnetic fields due to the unfavourable field dependence of the cross-effect mechanism. For example, in a 3.2 mm rotor, the ^{1}H enhancement factor of a frozen solution of 10 mM AMUPol in d_8-glycerol/D_2O/H_2O 60/30/10 (v/v/v) drops from ε = 250 at 9.4 T, to ~140 at 14.1 T, 48 at 18.8 T and 20 at 21.1 T (Lund et al., 2020). To overcome this problem, a group of water-soluble binitroxide polarising agents known as TinyPols (**18**) were developed, which have a three-bond non-conjugated flexible amine linker that allows substantial couplings between the two unpaired electrons. When the distance between the two unpaired electrons on TinyPols was reduced, the unfavourable field dependence was significantly reduced compared to AMUPol. The best performing polarising agent in this series was M-TinyPol (**19**), which produced DNP enhancement factors of ε = 90 and 38 at 18.8 T and 21.1 T, respectively [116].

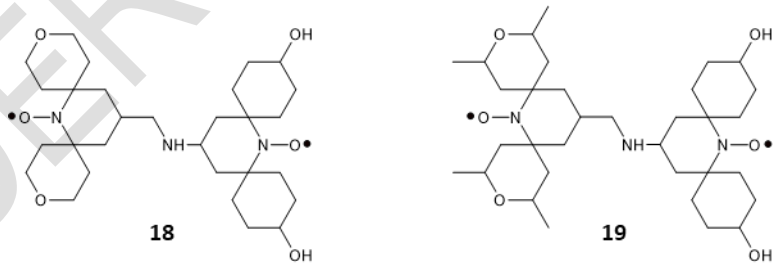

M-TinyPol at a concentration of 10 mM was used to achieve a 22-fold DNP enhancement in ^{13}C spectra of [1,3-$^{13}C_2$/2-^{13}C/^{15}N]-labeled amyloid Aβ1-42 at high magnetic field (18.8 T). This enabled the acquisition of well-resolved and sensitive two-dimensional and three-dimensional correlation spectra and nearly complete resonance assignment of the core of M0Aβ1-42 (K16-A42) using sub milligram sample quantities (Fig. 7). Many unambiguous internuclear proximities were detected, which defined the structure of the core and the arrangement of the different monomers [117].

3.8 Verdazyl-ribose

The water-soluble monoradical verdazyl-ribose (**20**) was synthesised in two steps by condensation of 2,4-diisopropylcarbonobis(hydrazide) bis-hydrochloride with ribose [118] and later tested as a potentially useful polarising

agent for DNP-ssNMR. With a sample of [^{15}N,$^{13}C_3$]-*L*-alanine at 31 K, a concentration of 40 mM verdazyl-ribose produced DNP enhancement factors of ε = 31 and 74 in ^{13}C spectra with MAS (6.7 kHz) and without MAS, respectively [119].

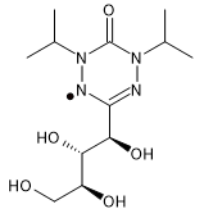

20

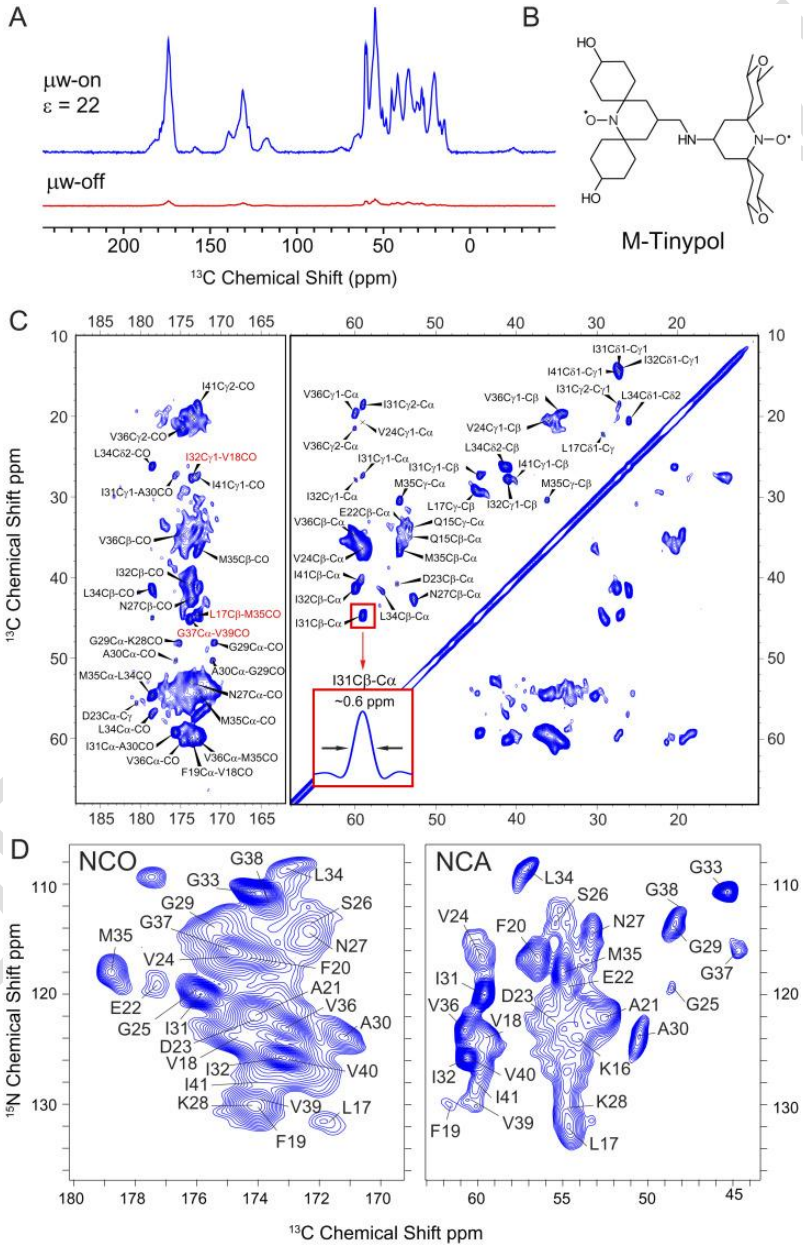

Fig. 7. (A) DNP-enhanced ^{13}C spectra of 1,3-$^{13}C_2$/2-^{13}C/^{15}N-labeled M0Aβ1-42 illustrating and enhancement of ε = 22 using (B) bis-nitroxide polarising agent M-TinyPol (**19**). (C) DNP-enhanced ^{13}C-^{13}C CORD-RFDR spectra of 1,3-$^{13}C_2$/2-^{13}C/^{15}N-labeled M0Aβ1-42. The resolution in the spectrum is comparable to that obtained at ambient temperatures, ~0.6 ppm as indicated for I31Cβ-Cα. In red are shown the long-range contacts that correspond to the intramolecular monomer

structure of the fibril. (D) DNP-enhanced NCO and NCA (Right) spectra acquired using M-TinyPol as the polarising agent. ωr/2π = 40 kHz and T = 115 K. This figure was reproduced from Bahri et al. (2022) [117].

3.9 Trityl radicals OX063 and StaPols

The trityl radical OX063 (**21**) (15 mM) was used as the polarising agent in DNP-ssNMR experiments at 1.4 K to enhance the signals for [1-^{13}C]lactate and [2-^{13}C]pyruvate in rat muscle. A DNP enhancement of ε = ~28 enabled measurement of the rapid pyruvate and lactate kinetics [120]. The seven-step synthesis of OX063 was reported later [121].

A series of biradical derivatives of OX063, known as StaPols, were synthesised to contain both the trityl radical and a nitroxide radical on a pyrroline group. To achieve this, OX063 was covalently conjugated with the highly stable gem-diethyl pyrroline nitroxide through a rigid piperazine linker. StaPol-1 (**22**) and StaPol-2 (**23**) were highly soluble and highly stable towards reducing agents [122]. DNP-ssNMR measurements on a sample containing 0.25 M [^{13}C, ^{15}N]proline and 10 mM biradical in d_8-glycerol/D_2O/H_2O, 60/30/10 (v/v/v) at high field (18.8 T) and 95 K produced high DNP enhancements of ε = 84, 105 and 117 for StaPol-2, StaPol-3 (**24**) and StaPol-1, respectively. Measurements on [^{13}C, ^{15}N]ubiquitin with 30 mM StaPol-1 in vitro, in HeLa cells and in cell lysate produced DNP enhancements of ε = 117, 50 and 183, respectively. The high stability and excellent DNP performance of StaPol-1 may originate from structural rigidity in the molecule [122].

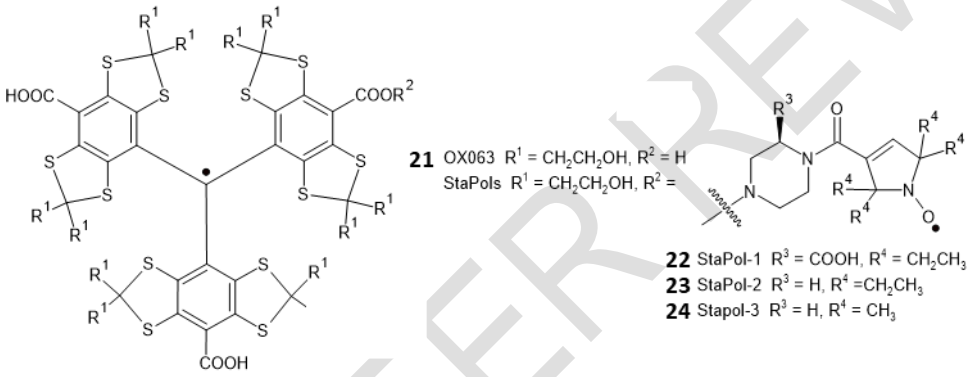

4. TARGETED POLARISING AGENTS AND SPIN TAGS

Whilst conventional polarising agents are mixed throughout the sample, others are targeted at specific sites to provide a more localised signal enhancement. In some cases, this allows samples to be matrix free to provide a more concentrated sample. Polarising agents can also be covalently linked in the sample to provide highly specific spin tags.

4.1 Membrane-anchored biradicals

A series of biradical polarising agents was developed for DNP-ssNMR investigation of matrix-free supported lipid bilayer samples. This included the agents bTurea-C16 (**25**), PyPol-C16 (**26**), and PyPol-cholesterol (**27**), which were designed to mimic lipid molecules and be membrane-anchored [123]. When PyPol-C16 was used with static samples of the antimicrobial peptide PGLa oriented in DMPC/DMPG lipids at 100 K, a DNP enhancement factor of ε = 17 was achieved [124].

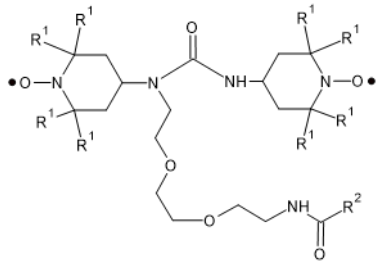

4.2 TotaFAM

The large trimodal fluorescent polarising agent TotaFAM (**28**) contains a maleimide-derived TOTAPOL for cross effect DNP, a Tat peptide (residues 47–57 of the HIV-1 Tat protein) for intracellular targeting, and a fluorophore (6-FAM) for optical localisation. TotaFAM was used at 2.7 mM in ^{13}C-enriched intact human embryonic kidney cells (HEK293F) at ultra-low temperatures of <6 K to achieve a DNP enhancement of ε = 63 in ^{13}C spectra [125]. Such polarising agents enable the subcellular localisation determined by optical microscopy to be correlated with chemical and structural information determined by in cell DNP-ssNMR.

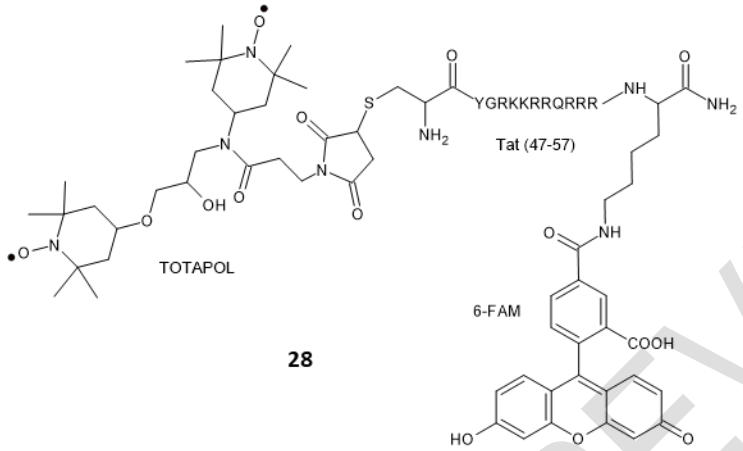

28

4.3 Site-specific spin labelling at disulphide bridges

A strategy for site-specific spin labelling at disulphide bridges in bioactive molecules was demonstrated with the cyclic heptapeptide eptifibatide (deam-ino-cysteinyl-*DL*-homoarginyl-glycyl-*DL*-alpha-aspartyl-*DL*-tryptophyl-*DL*-prolyl-*DL*-cysteinamide (1->7)-disulfide), which is an antiplatelet aggregation inhibitor deriving from the venom of rattlesnakes [126]. A bis-sulfone based spin label containing a TEMPO group (**29**) was synthesised in three-steps starting from 4-acetylbenzoic acid. The spin label was intercalated in eptifibatide by Michael reaction of its allylsulfone form with the reduced form (disulphide bond opened by DTT) of eptifibatide. The radical properties of the spin-labelled eptifibatide were confirmed by EPR spectroscopy, then ^{1}H/^{13}C DNP measurements were performed on 15 mM spin-labelled eptifibatide in a 8.2 M glycerol-d_8/D_2O/H_2O matrix at 97/107 K. Based on the signals originating from glycerol, there were DNP enhancements of ε = 14 and 19 in ^{1}H and ^{1}H-^{13}C CP spectra, respectively [126].

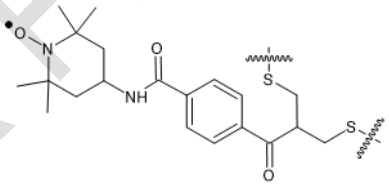

29

4.4 Targeted TOTAPOL

In some types of samples for ssNMR, polarising agents such as TOTAPOL (**4**) can be targeted in the sample, rather than dispersed throughout it, by exploiting the natural affinity of TOTAPOL for sugar-like moieties. This approach has been used with samples of cellulose and *Bacillus subtilis* bacterial cells (targeting the peptidoglycan layer) to achieve DNP enhancements at 100 K of ε = 20 and 24, respectively [127,128]. The “gluing agents” glucose/trehalose can also be used as an adhesive to stick TOTAPOL to the surface of a protein to prevent its aggregation, which has been demonstrated on lysozyme [128]. In a similar manner, the affinity of TOTAPOL to amyloid surfaces was exploited to assist structural investigations of CsgA amyloid fibrils from *Escherichia coli* by DNP-ssNMR [129]. Furthermore, the concept of sedimented solute DNP (SedDNP) was introduced, whereby the polarising agent is co-sedimented with the protein in the absence of a glass-forming agent. This approach was demonstrated using TOTAPOL (2-15 mM) with the iron-storage protein complex apoferritin (ApoF) and with bovine serum albumin (Fig. 8) at <90 K to achieve DNP enhancements in ^{13}C spectra of ε = 42 and 66, respectively [88,130]. The targeted approach allows matrix-free sample preparation (i.e., no solvent or cryoprotectant), which has the advantages of avoiding line-broadening interactions and maximising the sample filling factor, thus significantly reducing the time for acquiring correlation spectra.

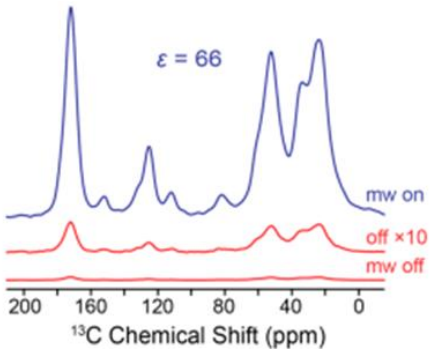

Fig. 8. DNP-enhanced ("mw on", blue) and thermal equilibrium ("mw off", red) polarisation ^{13}C-CPMAS spectrum of natural abundance bovine serum albumin sedimented from a 100 mg/mL solution in 90/10 (v/v) D_2O/H_2O with 5 mM TOTAPOL (**4**). The thermal equilibrium spectrum has also been multiplied by a factor of 10 ("off × 10", red) for better comparison. This figure was reproduced from Ravera et al. (2014) [88].

4.5 Covalently bound spin labels

A polarising group can be unambiguously targeted in the DNP-ssNMR sample by covalently binding it to the biological molecule of interest. For example, a nitroxide spin label at the N-terminus intermolecular interface region of Gramicidin became proximal only when channels formed in the membrane and produced DNP enhancements of up to ε = 6 for the dimeric protein in lipid bilayers at 115-120 K [131].

A TOTAPOL-derived spin tag, ToSMTSL (**30**), containing a methanethiosulfonate group (−SSO_2CH_3) that can react selectively with the thiol group of exposed cysteine residues on a protein, was synthesised from TOTAPOL. ToSMTSL was covalently linked to [U-^{15}N]-labelled cysteine mutants (N148C and S26C) of Anabaena sensory rhodopsin reconstituted in DMPC:DMPA liposomes. Such samples produced ^{15}N spectra with DNP enhancements of up to ε = 15. Whilst this was similar to DNP enhancements from samples co-suspended with TOTAPOL (~17 mM) in glycerol-d_8/D_2O/H_2O, the sensitivity possible with ToSMTSL would be four-fold greater due to the gain in filling factor [132]. In further work, ToSMTSL was conjugated with the sulfhydryl group of 1,2-dipalmitoyl-sn-glycero-3-phosphothioethanol (PTE) to obtain a lipid with a biradical-modified head group. The resultant ToSMTSL-PTE (**31**) was reconstituted in lipid bi-layers and used to polarise lipid-embedded [U-^{13}C]-labelled proteorhodopsin at 102 K to give DNP enhancements in ^{13}C spectra of up to ε = 7 [133].

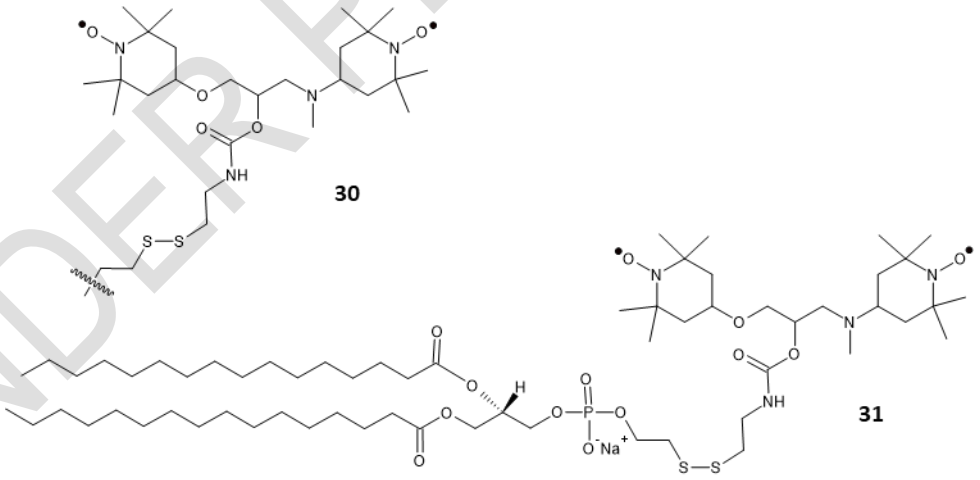

A maleimide-modified TOTAPOL radical (mTP) (**32**) was synthesised from TOTAPOL by acylating the secondary amino group on the linker connecting the two TEMPO units. An N-terminally cysteinylated Bak-derived peptide was then ligated with mTP. By performing DNP-ssNMR experiments at 108 K on [U-^{13}C, ^{15}N]-labelled Bcl-xL tagged with mTP in cell lysates, it was possible to selectively enhance the signals for the Bak peptide over those from other cell components [134]. Subtraction of the background signal (from a sample without the selective Bak peptide) enabled acquisition of DNP-enhanced 2D spectra of Bcl-XL in cell extracts prepared from cells grown in [U-^{13}C, ^{15}N)-labelled media. Indeed, this approach used approximately 400-fold less radicals to achieve a similar signal enhancement compared to conventional experiments with non-targeted TOTAPOL [134].

A nanomolar affinity ligand of dihydrofolate reductase (DHFR), trimethoprim, was covalently linked to TOTAPOL to create the derivatised polarising agent TMP-T (**33**). When TMP-T was bound to DHFR, DNP enhancements of up to $\varepsilon = 42$ in ^{13}C spectra were achieved at 100-110 K, which was comparable to using TOTAPOL co-dissolved with the protein [135].

An AMUPol-derived spin tag, AMUPol-MTSSL (**34**), was synthesised and covalently linked to the KcsA ion channel. Sedimented samples of KcsA-MTSSL in liposomes produced ^{13}C spectra with DNP enhancement factors of $\varepsilon = 12\text{-}15$ [136].

32

34

33

A functionalised ligand composed of *D*-galactose, a phenylglycine linker and TOTAPOL (**35**) was used as a paramagnetic tag to probe the ligand binding site of the galactophilic lectin LecA. At 100 K, DNP enhancements in ^{13}C spectra of up to $\varepsilon = 43$ were achieved, which enabled acquisition of well-resolved correlation spectra to measure interactions between LecA residues and *D*-galactose (Fig. 9) [137]. Because this approach allowed selective highlighting and identification of residues present in the binding site, the authors called this method Selective Dynamic Nuclear Polarisation. In Sel-DNP two datasets of each ssNMR experiment must be recorded, a reference set for the biomolecular bound-ligand complex for which the polarising agent is homogeneously distributed in the sample, and a second spectrum obtained with the same pulse sequence, but using a specific ligand tethered to a paramagnetic tag [137]. An advantage of Sel-DNP is that it does not have a limitation to the size of the biomolecular target that can be studied, because only residues close to the ligand–polarisation tag are detected.

35

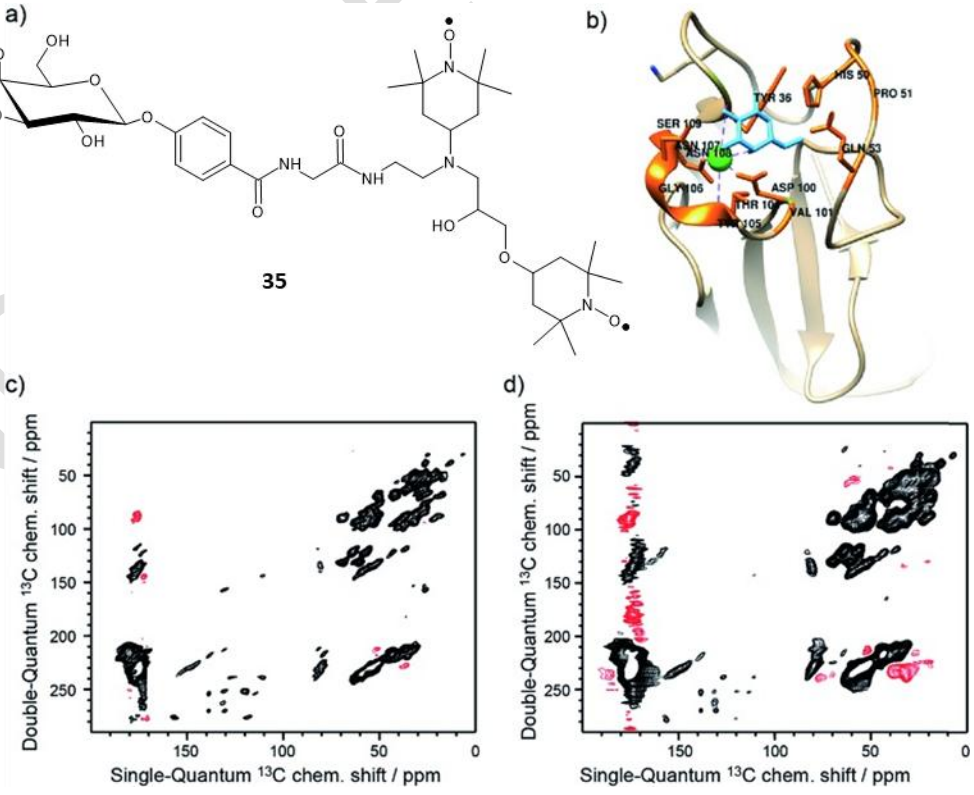

Fig. 9. Legend. (a) Functionalised ligand used in Sel-DNP and composed of a ligand tethered to a paramagnetic tag via a short linker (**35**). The ligand corresponds to *D*-galactose, the linker is made of a phenylglycine unit, and the paramagnetic tag is the bis-nitroxide TOTAPOL. (b) Structure of the binding site of LecA highlighting the residues known (from the crystal structure) to interact with the galactose ligand (in cyan). (c) and (d) DNP-enhanced ^{13}C–^{13}C DQ/SQ one-bond correlation spectra of LecA, using (c) AMUPol (reference spectrum S0) and (d) the functionalized ligand of (a) (spectrum S). Positive contours are in black and negative ones are in red. This figure was adapted from Marin-Montesinos et al. (2019) [137].

In a novel targeted approach, proteins were engineered to contain the unnatural amino acid norbornene-lysine (**36**), containing a strained cycloalkene group. The cycloalkene was selectively reacted with a tetrazine group on a TOTAPOL-derived polarising agent (**37**). Norbornene-lysine was incorporated into the three proteins ubiquitin, heterochromatin protein 1 (HP1α) and the structural maintenance of chromosomes (SMC) protein from *Pyrococcus yayanosii* using an orthogonal tRNA and aminoacyl-tRNA synthetase (aaRS) pair introduced into the cell through a separate plasmid construct [138]. In ^{13}C DNP-ssNMR spectra of the ^{13}C-labelled proteins tagged with TOTAPOL-tetrazine at 100 K, DNP enhancements of ε = 24, 6 and 7 were achieved for ubiquitin, HP1α and SMC, respectively. The DNP enhancement provided by 1 mM tagged ubiquitin was 68% of that provided by dispersed TOTAPOL at 15 mM with untagged ubiquitin under the same conditions, and it was possible to record a 2D ^{13}C-^{13}C spectrum of 100 ug of tagged ubiquitin (1 mM) in less than a day [138].

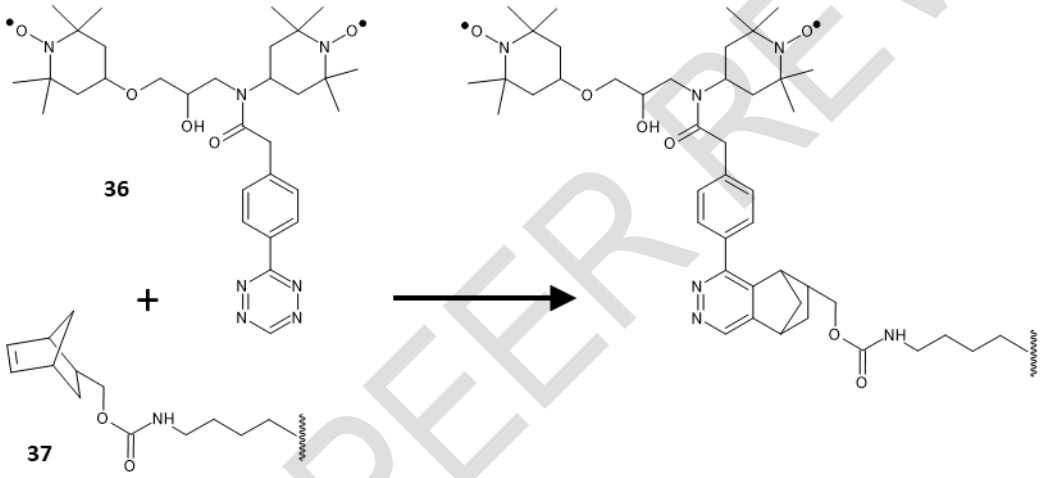

4.6 Spin-labelled peptides

Nitroxide-tagged peptides based on the 21-residue antimicrobial peptide maculatin 1.1 (Mac1) from the skin glands of an Australian tree frog (*Litoria genimaculata*) were used as a polarising agent for DNP-ssNMR studies in lipid membranes. The mutant F3W of Mac1 (MacW) was used and a single (T-MacW) and double (T-T-MacW) TOAC (2,2,6,6-tetramethylpiperidine-N-oxyl-4-amino-4-carboxylic acid) group was introduced at the C-terminus by solid-phase peptide synthesis to provide the spin-labelled peptides [139,140]. Because Mac1 has shown membrane-anchoring properties in lipid and bacterial membranes, it has the potential to selectively provide DNP enhancement to NMR signals from the membrane and from components (e.g. proteins) embedded within it. DNP enhancement properties of the spin-labelled peptides were assessed by adding [^{13}C-V14, ^{15}N-A18]-labelled Mac1 to DMPC bilayers in the presence of T-MacW or T-T-MacW, then ^{1}H-^{13}C and ^{1}H-^{31}P CP-MAS spectra were recorded at 108 K. There was an almost doubling of DNP enhancement produced by T-T-MacW compared to T-MacW. For example, ε = 13.7-14.4 for T-MacW and 22.1-27.0 for T-T-MacW in ^{13}C spectra, and ε = 12.0 for T-MacW and 19.4 for T-T-MacW in ^{31}P spectra [140].

4.7 Spin-labelled lipids

The spin-labelled lipids TEMPO-PC (1-palmitoyl-2-oleoyl-sn-glycero-3-phospho(tempo)-choline) (**38**), 7-Doxyl-PC (1-palmitoyl-2-stearoyl-(7-doxyl)-sn-glycero-3-phosphocholine) (**39**), and 16-Doxyl-PC (1-palmitoyl-2-stearoyl-(16-doxyl)-sn-glycero-3-phosphocholine) (**40**) have been investigated as polarising agents for DNP-ssNMR [141]. For these nitroxide monoradical-tagged lipids, it was found that the position of attachment for the nitroxide to the lipid molecule affects the DNP enhancement, where the enhancement decreased as the radical was positioned more deeply into the membrane (at 3 mol%). TEMPO-PC therefore produced the greatest enhancement. It was also found that when the spin-labelled lipid

concentration was increased beyond 3 mol%, the electron-electron dipolar interaction begins to interfere with DNP through the cross effect, so 3 mol%, was used as the optimum concentration [141]. In a separate study, TEMPO-PC and 5-Doxyl-PC were used to enhance ^{13}C spectra of the lipophilic lung surfactant mimetic peptide KL4 (KLLLLKLLLLKLLLLKLLLLK), which was $^{13}C'$-enriched at leucine 12. With KL4 in DPPC-d_{62}:POPG multilamellar vesicles, DNP enhancements of ε = 5.8-8.6 were achieved [142]. A lipid-anchored polarising agent N-propyl-PALMIPOL, which consists of a TOTAPOL moiety functionalized with a palmitate (C16) chain, was synthesised and used in DNP-ssNMR measurements with egg PC vesicles. The polarising agent is localised in the lipid bilayer with the biradical function at the surface of the liposomes and DNP experiments can be performed without excess cryo-protectant molecules. DNP enhancements of 2.7-8.1-fold in ^{13}C spectra were achieved [143]. An advantage of using spin-labelled lipids as the polarising agent is that no manipulation of the membrane protein is required.

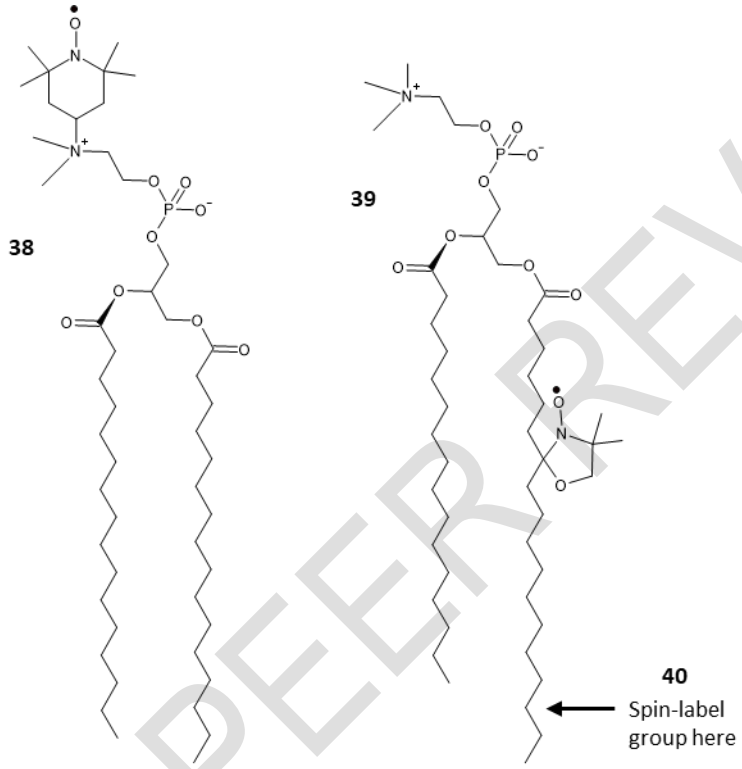

4.8 Endogenous radicals and paramagnetic metal ions

An endogenous stable radical of the flavin mononucleotide semiquinone of flavodoxin was used for DNP enhancement of ^{1}H ssNMR spectra at 90 K by a factor of 15-fold [144]. The endogenously bound paramagnetic metal ion Mn^{2+} cofactor in the [^{13}C, ^{15}N]-labelled full-length hammerhead ribozyme complex was used to enhance polarisation in DNP-ssNMR spectra without addition of any other polarising agent. A DNP enhancement of ε = 8 in ^{13}C spectra was achieved, which allowed acquisition of two-dimensional ^{15}N-^{13}C TEDOR and ^{13}C-^{13}C PDSD correlation spectra [145]. Overlap in these spectra was simplified by reducing the number of isotope-labelled nucleotides in the complex. This was achieved by spontaneous hybridization of two differently iso-tope-labelled strands, each individually synthesised by in-vitro transcription. Different isotope-labelling schemes allowed measurement of some inter-nucleotide distances [146].

Complexes of the paramagnetic metal ions Gd^{3+} and Mn^{2+} were investigated as polarising agents for DNP-ssNMR of ^{1}H, ^{13}C, and ^{15}N at magnetic fields of 5, 9.4, and 14.1 T. Then in preliminary DNP experiments on a protein, the Gd^{3+}-binding chelator tags DOTA-M (1,4,7,10-tetraazacyclododecane-1,4,7-tris-acetic acid-10-maleimidoethylacetamide) and 4MMDPA (4-mercaptomethyl dipicolinic acid) were attached to three single-site cysteine mutants (F4C, A28C, and G75C) of ubiquitin, which does not contain native cysteine residues [147]. Direct DNP-enhancement of ^{13}C in the [U-^{13}C, ^{15}N]-labelled A28C ubiquitin mutant with the Gd-DOTA-M (**41)** and Gd-4MMDPA (**42**) tags in [d_8,$^{12}C_3$]-glycerol/D_2O produced small and inverse enhancements by Gd^{3+} of ε = -0.8 to -1.2 and -1.7 to -3.1, respectively. Interestingly, when glycerol was absent from the sample, DNP enhancement factors improved three-fold. For example, in ^{13}C spectra of the [U-^{13}C, ^{15}N]-labelled F4C mutant labelled with Gd-DOTA-M, DNP enhancements were approximately ε = -3 and -9 in the presence and absence of glycerol, respectively. There was however line broadening in the presence of Gd^{3+}, which would make the extraction of structural information more challenging [147]. In more extensive experiments, perdeuteration of the protein to counteract nuclear spin-lattice relaxation and proton-driven spin diffusion effects improved DNP enhancements of ^{13}C

spectra, but only up to around ten-fold [148]. Direct DNP of ^{15}N nuclei produced much larger signal enhancements. For example, the 90% deuterated G75C mutant tagged with Gd-DOTA-M produced enhancements of >100-fold in the amide resonance. This approach enabled analysis of experimental DNP built-up dynamics, which was combined with structural modelling of the Gd^{3+}-tags in ubiquitin and provided quantitative information on the distance dependence of the initial DNP transfer [148].

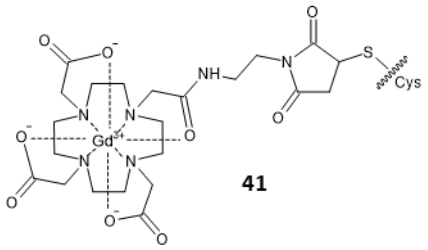

41

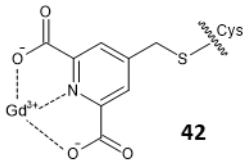

42

It was recently demonstrated that the commercially available and relatively inexpensive chemical gadolinium(III) nitrate [$Gd(NO_3)_3$] produces substantial DNP enhancements of ^{13}C and ^{15}N nuclei in [2-^{13}C, ^{15}N]glycine. A solution of 1.5 M [2-^{13}C, ^{15}N]glycine doped with 20 mM $Gd(NO_3)_3{\cdot}6H_2O$ in 1:3:6 (v/v/v) H_2O/D_2O/glycerol-d_8 produced direct NMR signal enhancements of $\varepsilon = -16$ (^{13}C) and –57 (^{15}N) and direct overall NMR signal enhancements of $\varepsilon = -35$ (^{13}C) and −197 (^{15}N) at 9.4 T and ~105 K [149]. The potential use of $Gd(NO_3)_3$ and other readily available simple metal-containing chemicals as polarising agents with different biological samples needs to be investigated.

5. CONCLUSION

One of the components required for performing DNP-ssNMR is a radical-containing polarising agent, and this usually must be an exogenous polarising agent that is added to the NMR sample. In these experiments the efficiency of polarisation transfer is highly dependent on the structure and chemical and physical properties of the polarising agent. In addition to providing efficient polarisation transfer, for biological samples the polarising agent must be soluble in the sample matrix and compatible with the biological sample, such that it does not adversely affect its native structure and function. The free radical(s) of the polarising agent also must be stable in the sample for the lifetime of DNP-ssNMR experiments. Appropriate tests and control experiments should be performed to assess the usefulness and compatibility of polarising agents with biological samples. Here we have reviewed the polarising agents and spin tags that have been used in DNP-ssNMR studies on biological samples. Nitroxides have been used most, especially the biradical compounds TOTAPOL and AMUPol and derivatives with a wide range of biological samples. In these experiments the three-spin cross effect mechanism of DNP transfer is dominant, but it is found that the enhancement efficiency of binitroxide polarising agents drops significantly at higher magnetic fields due to the unfavourable field dependence of the cross-effect mechanism. A balance between different sample and NMR conditions must therefore be assessed. Whilst conventional polarising agents are mixed throughout the sample, others are targeted at specific sites to provide a more localised signal enhancement. Targeted polarising agents enable use of matrix-free samples to concentrate the sample, whilst others can be covalently bound to provide signal enhancement at highly specific sites. The continued development of novel polarising agents and labelling and sample preparation strategies for DNP-ssNMR can open many biological samples to NMR studies that were not previously possible.

REFERENCES

1. Patching SG. NMR-active nuclei for biological and biomedical applications. Journal of Diagnostic Imaging in Therapy. 2016;3(1):7−48.
2. Bastawrous M, Jenne A, Tabatabaei Anaraki M, Simpson AJ. In-vivo NMR spectroscopy: A powerful and complimentary tool for understanding environmental toxicity. Metabolites. 2018;8(2):35.
3. Nitsche C, Otting G. NMR studies of ligand binding. Curr Opin Struct Biol. 2018;48:16−22.
4. Pandya A, Howard MJ, Zloh M, Dalby PA. An evaluation of the potential of NMR spectroscopy and computational modelling methods to inform biopharmaceutical formulations. Pharmaceutics. 2018;10(4):165.
5. Hatzakis E. Nuclear magnetic resonance (NMR) spectroscopy in food science: A comprehensive review. Compr Rev Food Sci Food Saf. 2019;18(1):189−220.
6. Zia K, Siddiqui T, Ali S, Farooq I, Zafar MS, Khurshid Z. Nuclear magnetic resonance spectroscopy for medical and dental applications: A comprehensive review. Eur J Dent. 2019;13(1):124−8.
7. Softley CA, Bostock MJ, Popowicz GM, Sattler M. Paramagnetic NMR in drug discovery. J Biomol NMR. 2020;74(6-7):287−309.

8. Anaraki MT, Lysak DH, Downey K, Kock FVC, You X, Majumdar RD et al. NMR spectroscopy of wastewater: A review, case study, and future potential. Prog Nucl Magn Reson Spectrosc. 2021;126-7:121−80.
9. Hansen PE. NMR of natural products as potential drugs. Molecules. 2021;26(12):3763.
10. Hu Y, Cheng K, He L, Zhang X, Jiang B, Jiang L et al. NMR-based methods for protein analysis. Anal Chem. 2021;93(4):1866−79.
11. Elsayed M, Isah A, Hiba M, Hassan A, Al‐ Garadi, K, Mahmoud M et al. A review on the applications of nuclear magnetic resonance (NMR) in the oil and gas industry: Laboratory and field-scale measurements. J Petrol Explor Prod Technol. 2022;12:2747–84.
12. Huang K, Thomas N, Gooley PR, Armstrong CW. Systematic review of NMR-based metabolomics practices in human disease research. Metabolites. 2022;12(10):963.
13. Sobolev AP, Ingallina C, Spano M, Di Matteo G, Mannina L. NMR-based approaches in the study of foods. Molecules. 2022;27(22):7906.
14. Patching SG. Solid-state NMR structures of integral membrane proteins. Mol Membr Biol. 2015;32(5-8):156−78.
15. Ladizhansky V. Applications of solid-state NMR to membrane proteins. Biochim Biophys Acta Proteins Proteom. 2017;1865(11 Pt B):1577−86.
16. Molugu TR, Lee S, Brown MF. Concepts and methods of solid-state NMR spectroscopy applied to biomembranes. Chem Rev. 2017;117(19):12087−132.
17. Demers JP, Fricke P, Shi C, Chevelkov V, Lange A. Structure determination of supra-molecular assemblies by solid-state NMR: Practical considerations. Prog Nucl Magn Reson Spectrosc. 2018;109:51−78.
18. Bonaccorsi M, Le Marchand T, Pintacuda G. Protein structural dynamics by magic-angle spinning NMR. Curr Opin Struct Biol. 2021;70:34−43.
19. Porat-Dahlerbruch G, Goldbourt A, Polenova T. Virus structures and dynamics by magic-angle spinning NMR. Annu Rev Virol. 2021;8(1):219−37.
20. Xue K, Movellan KT, Zhang XC, Najbauer EE, Forster MC, Becker S et al. Towards a native environment: structure and function of membrane proteins in lipid bilayers by NMR. Chem Sci. 2021;12(43):14332−42.
21. Ahlawat S, Mote KR, Lakomek NA, Agarwal V Solid-state NMR: Methods for biological solids. Chem Rev. 2022;122(10):9643−737.
22. Chandler B, Todd L, Smith SO. Magic angle spinning NMR of G protein-coupled receptors. Prog Nucl Magn Reson Spectrosc. 2022;128:25−43.
23. Ghassemi N, Poulhazan A, Deligey F, Mentink-Vigier F, Marcotte I, Wang T. Solid-state NMR investigations of extracellular matrixes and cell walls of algae, bacteria, fungi, and Plants. Chem Rev. 2022;122(10):10036−86.
24. Overhauser AW. Polarization of nuclei in metals. Phys Rev. 1953;92:411−5.
25. Carver TR, Slichter CP. Polarization of nuclear spins in metals. Phys Rev. 1953;92(1):212–3.
26. Wind RA, Duijvestijn MJ, Lugt CVD, Manenschijn A, Vriend J. Applications of dynamic nuclear polarization in ^{13}C NMR in solids. J Prog Nucl Magn Reson Spectrosc. 1985;17:33–67.
27. Singel DJ, Seidel DJ, Kendrick RD, Yannoni CS. A spectrometer for EPR, DNP, and multinuclear high-resolution NMR. J Magn Reson. 1989;81(1):145–61.
28. Afeworki M, McKay RA, Schaefer J. Selective observation of the interface of heterogeneous polycarbonate/polystyrene blends by dynamic nuclear polarization carbon-13 NMR spectroscopy. Macromolecules. 1992;25(16):4084–91.
29. Farrar CT, Hall DA, Gerfen GJ, Rosay M, Ardenkjaer-Larsen JH, Griffin RG. High-frequency dynamic nuclear polarization in the nuclear rotating frame. J Magn Reson. 2000;144(1):134−41.
30. Rosay M, Weis V, Kreischer KE, Temkin RJ, Griffin RG. Two-dimensional ^{13}C-^{13}C correlation spectroscopy with magic angle spinning and dynamic nuclear polarization. J Am Chem Soc. 2002;124(13):3214−5.
31. Bajaj VS, Farrar CT, Hornstein MK, Mastovsky I, Vieregg J, Bryant J et al. Dynamic nuclear polarization at 9T using a novel 250 GHz gyrotron microwave source. J. Mag. Res. 2003, 160, 85–90.
32. Rosay M, Lansing JC, Haddad KC, Bachovchin WW, Herzfeld J, Temkin RJ. High frequency dynamic nuclear polarization in MAS spectra of membrane and soluble proteins. J Am Chem Soc. 2011;213(2):404-9.
33. Hu KN, Yu HH, Swager TM, Griffin RG. Dynamic nuclear polarization with biradicals. J Am Chem Soc. 2004;126(35):10844−5.
34. Woskov PP, Bajaj VS, Hornstein MK, Temkin RJ, Griffin RG. Corrugated waveguide and directional coupler for CW 250-GHz gyrotron DNP experiments. IEEE Trans Microw Theory Tech. 2005;53(6):1863−9.
35. Song C, Hu KN, Joo CG, Swager TM, Griffin RG. TOTAPOL – A biradical polarizing agent for dynamic nuclear polarization experiments in aqueous media. J Am Chem Soc. 2006;128(35):11385–90.
36. Bajaj VS, Hornstein MK, Kreischer KE, Sirigiri JR, Woskov PP, Mak-Jurkauskas ML et al. 250GHz CW gyrotron oscillator for dynamic nuclear polarization in biological solid state NMR. J Magn Reson. 2007;189(2):251−79
37. Hu KN, Bajaj VS, Rosay M, Griffin RG. High frequency dynamic nuclear polarization using mixtures of TEMPO and trityl radicals. J Chem Phys. 2007;126(4):044512.
38. Maly T, Debelouchina GT, Bajaj VS, Hu KN, Joo CG, Mak-Jurkauskas ML et al. Dynamic nuclear polarization at high magnetic fields. J Chem Phys. 2008;128(5):052211.

39. Barnes AB, Paëpe GD, van der Wel PC, Hu KN, Joo CG, Bajaj VS et al. High-field dynamic nuclear polarization for solid and solution biological NMR. Appl Magn Reson. 2008;34(3-4):237−3.
40. Bajaj VS, Mak-Jurkauskas ML, Belenky M, Herzfeld J, Griffin RG. Functional and shunt states of bacteriorhodopsin resolved by 250 GHz dynamic nuclear polarization-enhanced solid-state NMR. Proc Natl Acad Sci U S A. 2009;106(23):9244–9
41. Griffin RG. Dynamic nuclear polarization at 9T using a novel 250 gyrotron microwave source. J Magn Reson. 2011;213(2):410−2.
42. Barnes AB, Markhasin E, Daviso E, Michaelis VK, Nanni EA, Jawla SK et al. Dynamic nuclear polarization at 700 MHz/460 GHz. J Magn Reson. 2012;224:1−7.
43. Ni QZ, Daviso E, Can TV, Markhasin E, Jawla SK, Swager TM et al. High frequency dynamic nuclear polarization. Acc Chem Res. 2013;46(9):1933−41.
44. Michaelis VK, Ong TC, Kiesewetter MK, Frantz DK, Walish JJ, Ravera E. Topical developments in high-field dynamic nuclear polarization. Isr J Chem. 2014;54(1-2):207−21.
45. Mathies G, Caporini MA, Michaelis VK, Liu Y, Hu KN, Mance D et al. Efficient dynamic nuclear polarization at 800 MHz/527 GHz with trityl-nitroxide biradicals. Angew Chem Int Ed. 2015;54(40):11770−4.
46. Su Y, Andreas L, Griffin RG. Magic angle spinning NMR of proteins: High-frequency dynamic nuclear polarization and ^{1}H detection. Annu Rev Biochem. 2015;84:465−97.
47. Gerfen GJ, Becerra LR, Hall DA, Griffin RG, Temkin RJ, Singel DJ. High frequency (140 GHz) dynamic nuclear polarization: polarization transfer to a solute in frozen aqueous solution. J Chem Phys. 1995;102:9494.
48. Hall DA, Maus DC, Gerfen GJ, Inati SJ, Becerra LR, Dahlquist FW et al. Polarization-enhanced NMR spectroscopy of biomolecules in frozen solution. Science. 1997;276(5314):930−2
49. Golman K, Zandt RI, Lerche M, Pehrson R, Ardenkjaer-Larsen JH. Metabolic imaging by hyperpolarized ^{13}C magnetic resonance imaging for in vivo tumor diagnosis. Cancer Res. 2006;66(22):10855–60.
50. Akbey Ü, Oschkinat H. Structural biology applications of solid state MAS DNP NMR. J Magn Reson. 2016;269:213−24.
51. Itin B, Sergeyev IV. Strategies for efficient sample preparation for dynamic nuclear polarization solid-state NMR of biological macromolecules. Methods Mol Biol. 2018;1688:133−54.
52. Jaudzems K, Polenova T, Pintacuda G, Oschkinat H, Lesage A. DNP NMR of biomolecular assemblies. J Struct Biol. 2019;206(1):9−98.
53. Biedenbänder T, Aladin V, Saeidpour S, Corzilius B. Dynamic nuclear polarization for sensitivity enhancement in biomolecular solid-state NMR. Chem Rev. 2022;122(10):9738−94.
54. Chow WY, De Paëpe G, Hediger S. Biomolecular and biological applications of solid-state NMR with dynamic nuclear polarization enhancement. Chem Rev. 2022;122(10):9795−847.
55. Loening NM, Rosay M, Weis V, Griffin RG. Solution-state dynamic nuclear polarization at high magnetic field. J Am Chem Soc. 2002;124(30):8808–9.
56. Villanueva-Garibay JA, Annino G, van Bentum PJ, Kentgens AP. Pushing the limit of liquid-state dynamic nuclear polarization at high field. Phys Chem Chem Phys. 2010;12(22):5846−9
57. Ravera E, Luchinat C, Parigi G. Basic facts and perspectives of Overhauser DNP NMR. J Magn Reson. 2016;264:78−87.
58. Hu KN, Debelouchina GT, Smith AA, Griffin RG. Quantum mechanical theory of dynamic nuclear polarization in solid dielectrics. J Chem Phys. 2011;134(12):125105.
59. van Bentum J, van Meerten B, Sharma M, Kentgens A. Perspectives on DNP-enhanced NMR spectroscopy in solutions. J Magn Reson. 2016;264:59−67.
60. Hovav Y, Feintuch A, Vega S. Theoretical aspects of dynamic nuclear polarization in the solid state - the cross effect. J Magn Reson. 2012;214(1):29–41.
61. Jeffries C. Polarization of nuclei by resonance saturation in paramagnetic crystals. Phys Rev. 1957;106(1):164–5.
62. Abragam A, Proctor WG. Une nouvelle methode de polarisation dynamique des noyaux atomiques dans les solides. C R Hebd Seances Acad Sci. 1958;246:2253–6.
63. Becerra LR, Gerfen GJ, Temkin RJ, Singel DJ, Griffin, R.G. Dynamic nuclear polarization with a cyclotron resonance maser at 5 T. Phys Rev Lett. 1993;71(21):3561–4.
64. Hu KN, Bajaj VS, Rosay MM, Griffin RG. High frequency dynamic nuclear polarization using mixtures of TEMPO and trityl radicals. J Chem Phys. 2007;126(4):044512.
65. Haze O, Corzilius B, Smith AA, Griffin RG, Swager TM. Water-soluble narrow-line radicals for dynamic nuclear polarization. J Am Chem Soc. 2012;34(35):14287–90.
66. Kessenikh AV, Lushchikov VI, Manenkov AA, Taran YV. Proton polarization in irradiated polyethylenes. Sov Phys - Solid State. 1963;5:321−9.
67. Kessenikh AV, Luschikov VI, Manenkov AA. Dynamic polarization of nuclei during saturation of nonuniformly broadened electron paramagnetic resonance lines. Sov Phys - Solid State. 1963;5:835−7.
68. Kessenikh AV, Manenkov AA, Pyatnitskii GI. On explanation of experimental data on dynamic polarization of protons in irradiated polyethylenes. Sov Phys - Solid State 1964;6:641−3.

69. Hwang C, Hill D. Phenomenological model for the new effect in dynamic polarization. Phys Rev Lett. 1967;19:1011–4.
70. Corzilius B, Smith AA, Griffin RG. Solid effect in magic angle spinning dynamic nuclear polarization. J Chem Phys. 2012;137(5):054201.
71. Mentink-Vigier F, Akbey Ü, Oschkinat H, Vega S, Feintuch A. Theoretical aspects of magic angle spinning - dynamic nuclear polarization. J Magn Reson. 2015;258:102−20.
72. Corzilius B. Theory of solid effect and cross effect dynamic nuclear polarization with half-integer high-spin metal polarizing agents in rotating solids. Phys Chem Chem Phys. 2016;18(39):27190−204.
73. Lilly Thankamony AS, Wittmann JJ, Kaushik M, Corzilius B. Dynamic nuclear polarization for sensitivity enhancement in modern solid-state NMR. Prog Nucl Magn Reson Spectrosc. 2017;102−3:120−95.
74. Mak-Jurkauskas ML, Bajaj VS, Hornstein MK, Belenky M, Griffin RG, Herzfeld J. Energy transformations early in the bacteriorhodopsin photocycle revealed by DNP-enhanced solid-state NMR. Proc Natl Acad Sci U S A. 2008;105(3):883−8.
75. Dai D, Wang X, Liu Y, Yang XL, Glaubitz C, Denysenkov V et al. Room-temperature dynamic nuclear polarization enhanced NMR spectroscopy of small biological molecules in water. Nat Commun. 2021;12(1):6880.
76. Dollmann BC, Kleschyov AL, Sen V, Golubev V, Schreiber LM, Spiess HW. Spin-labeled heparins as polarizing agents for dynamic nuclear polarization. ChemPhysChem. 2010;11(17):3656−3663.
77. van der Wel PC, Hu KN, Lewandowski J, Griffin RG. Dynamic nuclear polarization of amyloidogenic peptide nanocrystals: GNNQQNY, a core segment of the yeast prion protein Sup35p. J Am Chem Soc. 2006;128(33):10840−6.
78. Debelouchina GT, Bayro MJ, van der Wel PC, Caporini MA, Barnes AB, Rosay M et al. Dynamic nuclear polarization-enhanced solid-state NMR spectroscopy of GNNQQNY nanocrystals and amyloid fibrils. Phys Chem Chem Phys. 2010;12(22):5911−9.
79. Bayro MJ, Debelouchina GT, Eddy MT, Birkett NR, MacPhee CE, Rosay M et al. Intermolecular structure determination of amyloid fibrils with magic-angle spinning and dynamic nuclear polarization NMR. J Am Chem Soc. 2011;133(35):13967−74.
80. Debelouchina GT, Bayro MJ, Fitzpatrick AW, Ladizhansky V, Colvin MT, Caporini MA et al. Higher order amyloid fibril structure by MAS NMR and DNP spectroscopy. J Am Chem Soc. 2013;135(51):19237−47.
81. Frederick KK, Michaelis VK, Corzilius B, Ong TC, Jacavone AC, Griffin RG et al. Sensitivity-enhanced NMR reveals alterations in protein structure by cellular milieus. Cell. 2015;163(3):620−8.
82. Bajaj VS, Mak-Jurkauskas ML, Belenky M, Herzfeld J, Griffin RG. Functional and shunt states of bacteriorhodopsin resolved by 250 GHz dynamic nuclear polarization-enhanced solid-state NMR. Proc Natl Acad Sci U S A. 2009;106(23):9244−9.
83. Akbey Ü, Franks WT, Linden A, Lange S, Griffin RG, van Rossum BJ et al. Dynamic nuclear polarization of deuterated proteins. Angew Chem Int Ed. 2010;49(42):7803−6.
84. Linden AH, Lange S, Franks WT, Akbey U, Specker E, van Rossum BJ et al. Neurotoxin II bound to acetylcholine receptors in native membranes studied by dynamic nuclear polarization NMR. J Am Chem Soc. 2011;133(48):19266−9.
85. Reggie L, Lopez JJ, Collinson I, Glaubitz C, Lorch M. Dynamic nuclear polarization-enhanced solid-state NMR of a ^{13}C-labeled signal peptide bound to lipid-reconstituted Sec translocon. J Am Chem Soc. 2011;133(47):19084−6.
86. Wang T, Park YB, Caporini MA, Rosay M, Zhong L, Cosgrove DJ et al. Sensitivity-enhanced solid-state NMR detection of expansin's target in plant cell walls. Proc Natl Acad Sci U S A. 2013;110(41):16444−9.
87. Takahashi H, Ayala I, Bardet M, De Paëpe G, Simorre JP, Hediger S. Solid-state NMR on bacterial cells: selective cell wall signal enhancement and resolution improvement using dynamic nuclear polarization. J Am Chem Soc. 2013;135(13):5105−10.
88. Ravera E, Corzilius B, Michaelis VK, Luchinat C, Griffin RG, Bertini I. DNP-enhanced MAS NMR of bovine serum albumin sediments and solutions. J Phys Chem B. 2014;118(11):2957−65.
89. Smith AN, Caporini MA, Fanucci GE, Long JR. A method for dynamic nuclear polarization enhancement of membrane proteins. Angew Chem Int Ed. 2015;54(5):1542−6.
90. Lange S, Franks WT, Rajagopalan N, Döring K, Geiger MA, Linden A et al. Structural analysis of a signal peptide inside the ribosome tunnel by DNP MAS NMR. Sci Adv. 2016;2(8):e1600379.
91. Yamamoto K, Caporini MA, Im SC, Waskell L, Ramamoorthy A. Transmembrane interactions of full-length mammalian bitopic cytochrome-P450-cytochrome-b5 complex in lipid bilayers revealed by sensitivity-enhanced dynamic nuclear polarization solid-state NMR spectroscopy. Sci Rep. 2017;7(1):4116.
92. Andreas LB, Barnes AB, Corzilius B, Chou JJ, Miller EA, Caporini M et al. Dynamic nuclear polarization study of inhibitor binding to the M2(18-60) proton transporter from influenza A. Biochemistry. 2013;52(16):2774−82.
93. Ong YS, Lakatos A, Becker-Baldus J, Pos KM, Glaubitz C. Detecting substrates bound to the secondary multidrug efflux pump EmrE by DNP-enhanced solid-state NMR. J Am Chem Soc. 2013;135(42):15754−62.
94. Koers EJ, van der Cruijsen EA, Rosay M, Weingarth M, Prokofyev A, Sauvée C et al. NMR-based structural biology enhanced by dynamic nuclear polarization at high magnetic field. J Biomol NMR. 2014;60(2-3):157−68.

95. Gupta R, Zhang H, Lu M, Hou G, Caporini M, Rosay M et al. Dynamic nuclear polarization magic-angle spinning nuclear magnetic resonance combined with molecular dynamics simulations permits detection of order and disorder in viral assemblies. J Phys Chem B. 2019;123(24):5048−58.
96. McCoy KM, Rogawski R, Stovicek O, McDermott AE. Stability of nitroxide biradical TOTAPOL in biological samples. J Magn Reson. 2019;303:115−20.
97. Sauvée C, Rosay M, Casano G, Aussenac F, Weber RT, Ouari O et al. Highly efficient, water-soluble polarizing agents for dynamic nuclear polarization at high frequency. Angew Chem Int Ed. 2013;52(41):10858−61.
98. Elkins MR, Sergeyev IV, Hong M. Determining cholesterol binding to membrane proteins by cholesterol ^{13}C labeling in yeast and dynamic nuclear polarization NMR. J Am Chem Soc. 2018;140(45):15437−49.
99. Maciejko J, Kaur J, Becker-Baldus J, Glaubitz C. Photocycle-dependent conformational changes in the proteorhodopsin cross-protomer Asp-His-Trp triad revealed by DNP-enhanced MAS-NMR. Proc Natl Acad Sci U S A. 2019;116(17):8342−9.
100. Ghosh R, Dumarieh R, Xiao Y, Frederick KK. Stability of the nitroxide biradical AMUPol in intact and lysed mammalian cells. J Magn Reson. 2022;336:107150.
101. Jagtap AP, Geiger MA, Stöppler D, Orwick-Rydmark M, Oschkinat H, Sigurdsson ST. bcTol: A highly water-soluble biradical for efficient dynamic nuclear polarization of biomolecules. Chem Commun. (Camb.) 2016;52(43):7020−3.
102. Geiger MA, Jagtap AP, Kaushik M, Sun H, Stöppler D, Sigurdsson ST et al. Efficiency of water-soluble nitroxide biradicals for dynamic nuclear polarization in rotating solids at 9.4 T: bcTol-M and cyolyl-TOTAPOL as new polarizing agents. Chemistry. 2018;24(51):13485−94.
103. Stöppler D, Song C, van Rossum BJ, Geiger MA, Lang C, Mroginski MA et al. Dynamic nuclear polarization provides new insights into chromophore structure in phytochrome photoreceptors. Angew Chem Int Ed. 2016;55(52):16017−20.
104. Goldberga I, Li R, Chow WY, Reid DG, Bashtanova U, Rajan R et al. Detection of nucleic acids and other low abundance components in native bone and osteosarcoma extracellular matrix by isotope enrichment and DNP-enhanced NMR. RSC Adv. 2019;9(46):26686−90.
105. Thurber KR, Yau WM, Tycko R. Low-temperature dynamic nuclear polarization at 9.4T with a 30mW microwave source. J Magn Reson. 2010;204(2):303–13.
106. Potapov A, Yau WM, Tycko R. Dynamic nuclear polarization-enhanced ^{13}C NMR spectroscopy of static biological solids. J Magn Reson. 2013;231:5−14.
107. Yau WM, Thurber KR, Tycko R. Synthesis and evaluation of nitroxide-based oligoradicals for low-temperature dynamic nuclear polarization in solid state NMR. J Magn Reson. 2014;244:98−106.
108. Potapov A, Yau WM, Ghirlando R, Thurber KR, Tycko R. Successive stages of amyloid-β self-assembly characterized by solid-state nuclear magnetic resonance with dynamic nuclear polarization. J Am Chem Soc. 2015;137(25):8294−307.
109. Yau WM, Jeon J, Tycko R. Succinyl-DOTOPA: An effective triradical dopant for low-temperature dynamic nuclear polarization with high solubility in aqueous solvent mixtures at neutral pH. J Magn Reson. 2020;311:106672.
110. Salnikov E, Rosay M, Pawsey S, Ouari O, Tordo P, Bechinger B. Solid-state NMR spectroscopy of oriented membrane polypeptides at 100 K with signal enhancement by dynamic nuclear polarization. J Am Chem Soc. 2010;132(17):5940–1.
111. Craig HC, Blamires SJ, Sani MA, Kasumovic MM, Rawal A, Hook JM. DNP NMR spectroscopy reveals new structures, residues and interactions in wild spider silks. Chem Commun. (Camb.) 2019;55(32):4687−90.
112. Kiesewetter MK, Corzilius B, Smith AA, Griffin RG, Swager TM. Dynamic nuclear polarization with a water-soluble rigid biradical. J Am Chem Soc. 2012;134(10):4537−40.
113. Mentink-Vigier F, Marin-Montesinos I, Jagtap AP, Halbritter T, van Tol J, Hediger S et al. Computationally assisted design of polarizing agents for dynamic nuclear polarization enhanced NMR: The asymPol family. J Am Chem Soc. 2018;140(35):11013−9.
114. Ackermann BE, Lim BJ, Elathram N, Narayanan S, Debelouchina GT. A comparative study of nitroxide-based biradicals for dynamic nuclear polarization in cellular environments. ChemBiochem. 2022;23(24):e202200577.
115. Smith AN, Harrabi R, Halbritter T, Lee D, Aussenac F, van der Wel PCA et al. Fast magic angle spinning for the characterization of milligram quantities of organic and biological solids at natural isotopic abundance by ^{13}C-^{13}C correlation DNP-enhanced NMR. Solid State Nucl Magn Reson. 2023;123:101850.
116. Lund A, Casano G, Menzildjian G, Kaushik M, Stevanato G, Yulikov M et al. TinyPols: A family of water-soluble binitroxides tailored for dynamic nuclear polarization enhanced NMR spectroscopy at 18.8 and 21.1 T. Chem Sci. 2020;11(10):2810−8.
117. Bahri S, Silvers R, Michael B, Jaudzems K, Lalli D, Casano G et al. ^{1}H detection and dynamic nuclear polarization-enhanced NMR of Aβ1-42 fibrils. Proc Natl Acad Sci U S A. 2022;119(1):e2114413119.
118. Le TN, Grewal H, Changoco V, Truong V, Brook DJR. Water soluble, chiral, verdazyl radicals derived from aldoses. Tetrahedron. 2016;72(41):6368–74.
119. Thurber KR, Le TN, Changcoco V, Brook DJR. Verdazyl-ribose: A new radical for solid-state dynamic nuclear polarization at high magnetic field. J Magn Reson. 2018;289:122−31.

120. Park JM, Josan S, Mayer D, Hurd RE, Chung Y, Bendahan D et al. Hyperpolarized ^{13}C NMR observation of lactate kinetics in skeletal muscle. J Exp Biol. 2015;218(Pt 20):3308−18.
121. Poncelet M, Huffman JL, Khramtsov VV, Dhimitruka I, Driesschaert B. Synthesis of hydroxyethyl tetrathiatriarylmethyl radicals OX063 and OX071. RSC Adv. 2019;9(60):35073−35076.
122. Yao R, Beriashvili D, Zhang W, Li S, Safeer A, Gurinov A et al. Highly bioresistant, hydrophilic and rigidly linked trityl-nitroxide biradicals for cellular high-field dynamic nuclear polarization. Chem Sci. 2022;13(47):14157−64.
123. Salnikov ES, Aisenbrey C, Aussenac F, Ouari O, Sarrouj H, Reiter C et al. Membrane topologies of the PGLa antimicrobial peptide and a transmembrane anchor sequence by dynamic nuclear polarization/solid-state NMR spectroscopy. Sci Rep. 2016;6:20895.
124. Salnikov ES, Abel S, Karthikeyan G, Karoui H, Aussenac F, Tordo P et al. Dynamic nuclear polarization/solid-state NMR spectroscopy of membrane polypeptides: Free-radical optimization for matrix-free lipid bilayer samples. ChemPhysChem. 2017;18:2103−3.
125. Albert BJ, Gao C, Sesti EL, Saliba EP, Alaniva N, Scott FJ, et al. Dynamic nuclear polarization nuclear magnetic resonance in human cells using fluorescent polarizing agents. Biochemistry. 2018;57(31):4741−6.
126. Herr K, Fleckenstein M, Brodrecht M, Höfler MV, Heise H, Aussenac F et al. A novel strategy for site selective spin-labeling to investigate bioactive entities by DNP and EPR spectroscopy. Sci Rep. 2021;11(1):13714.
127. Takahashi H, Lee D, Dubois L, Bardet M, Hediger S, De Paëpe G et al. Rapid natural-abundance 2D ^{13}C-^{13}C correlation spectroscopy using dynamic nuclear polarization enhanced solid-state NMR and matrix-free sample preparation. Angew Chem Int Ed. 2012;51(47):11766–9.
128. Takahashi H, Hediger S, De Paëpe G. Matrix-free dynamic nuclear polarization enables solid-state NMR ^{13}C-^{13}C correlation spectroscopy of proteins at natural isotopic abundance. Chem Commun (Camb.) 2013;49(82):9479–81.
129. Nagaraj M, Franks TW, Saeidpour S, Schubeis T, Oschkinat H, Ritter C. Surface binding of TOTAPOL assists structural investigations of amyloid fibrils by dynamic nuclear polarization NMR spectroscopy. ChemBiochem. 2016;17(14):1308−11.
130. Ravera E, Corzilius B, Michaelis VK, Rosa C, Griffin RG, Luchinat C et al. Dynamic nuclear polarization of sedimented solutes. J Am Chem Soc. 2013;135(5):1641–4.
131. Wylie BJ, Dzikovski BG, Pawsey S, Caporini M, Rosay M, Freed JH et al. Dynamic nuclear polarization of membrane proteins: Covalently bound spin-labels at protein-protein interfaces. J Biomol NMR. 2015;61(3-4):361−7.
132. Voinov MA, Good DB, Ward ME, Milikisiyants S, Marek A, Caporini MA et al. Cysteine-specific labeling of proteins with a nitroxide biradical for dynamic nuclear polarization NMR. J Phys Chem B. 2015;119(32):10180−10190.
133. Good DB, Voinov MA, Bolton D, Ward ME, Sergeyev IV, Caporini M et al. A biradical-tagged phospholipid as a polarizing agent for solid-state MAS dynamic nuclear polarization NMR of membrane proteins. Solid State Nucl Magn Reson. 2019;100:92−101.
134. Viennet T, Viegas A, Kuepper A, Arens S, Gelev V, Petrov O et al. Selective protein hyperpolarization in cell lysates using targeted dynamic nuclear polarization. Angew Chem Int Ed. 2016;55(36):1–6.
135. Rogawski R, Sergeyev IV, Li Y, Ottaviani MF, Cornish V, McDermott AE. Dynamic nuclear polarization signal enhancement with high-affinity biradical tags. J Phys Chem B. 2017;121(6):1169–75.
136. van der Cruijsen EA, Koers EJ, Sauvée C, Hulse RE, Weingarth M, Ouari O et al. Biomolecular DNP-supported NMR spectroscopy using site-directed spin labeling. Chemistry. 2015;21(37):12971−7.
137. Marin-Montesinos I, Goyard D, Gillon E, Renaudet O, Imberty A, Hediger S. Selective high-resolution DNP-enhanced NMR of biomolecular binding sites. Chem Sci. 2019;10(11):3366−74.
138. Lim BJ, Ackermann BE, Debelouchina GT. Targetable tetrazine-based dynamic nuclear polarization agents for biological systems. ChemBiochem. 2020;21(9):1315−9.
139. Sani MA, Zhu S, Hofferek V, Separovic F. Nitroxide spin-labeled peptides for DNP-NMR in-cell studies. FASEB J. 2019;33(10):11021−7.
140. Zhu S, Kachooei E, Harmer JR, Brown LJ, Separovic F, Sani MA. TOAC spin-labeled peptides tailored for DNP-NMR studies in lipid membrane environments. Biophys J. 2021;120(20):4501−11.
141. Smith AN, Twahir UT, Dubroca T, Fanucci GE, Long JR. Molecular rationale for improved dynamic nuclear polarization of biomembranes. J Phys Chem B. 2016;120(32):7880−8.
142. Smith AN, Caporini MA, Fanucci GE, Long JR. A method for dynamic nuclear polarization enhancement of membrane proteins. Angew Chem Int Ed. 2015;54(5):1542−6.
143. Fernández-de-Alba C, Takahashi H, Richard A, Chenavier Y, Dubois L, Maurel V et al. Matrix-free DNP-enhanced NMR spectroscopy of liposomes using a lipid-anchored biradical. Chem - A Eur J. 2015;21(12):4512–4517.
144. Maly T, Cui D, Griffin RG, Miller AF. ^{1}H dynamic nuclear polarization based on an endogenous radical. J Phys Chem B. 2012;116(24):7055–7065.
145. Wenk P, Kaushik M, Richter D, Vogel M, Suess B, Corzilius B. Dynamic nuclear polarization of nucleic acid with endogenously bound manganese. J Biomol NMR. 2015;63(1):97−109.
146. Daube D, Vogel M, Suess B, Corzilius B. Dynamic nuclear polarization on a hybridized hammerhead ribozyme: An explorative study of RNA folding and direct DNP with a paramagnetic metal ion cofactor. Solid State Nucl Magn Reson. 2019;101:21−30.

147. Kaushik M, Bahrenberg T, Can TV, Caporini MA, Silvers R, Heiliger J et al. Gd(iii) and Mn(ii) complexes for dynamic nuclear polarization: small molecular chelate polarizing agents and applications with site-directed spin labeling of proteins. Phys Chem Chem Phys. 2016;18(39):27205-18.
148. Heiliger J, Matzel T, Çetiner EC, Schwalbe H, Kuenze G, Corzilius B. Site-specific dynamic nuclear polarization in a Gd(III)-labeled protein. Phys Chem Chem Phys. 2020;22(44):25455−66.
149. Elliott SJ, Duff BB, Taylor-Hughes AR, Cheney DJ, Corley JP, Paul S et al. Off-the-shelf $Gd(NO_3)_3$ as an efficient high-spin metal ion polarizing agent for magic angle spinning dynamic nuclear polarization. J Phys Chem B. 2022;126(33):6281−9.